

1 **Neuromuscular fatigue and recovery after strenuous exercise**  
2 **depends on skeletal muscle size and stem cell characteristics**

3 Baumert, P.<sup>1,2\*</sup>, Temple, S.<sup>1</sup>, Stanley, J.M.<sup>1</sup>, Cocks M.<sup>1</sup>, Strauss, J.A.<sup>1</sup>, Shepherd

4 S.O.<sup>1</sup>, Drust, B.<sup>1</sup>, Lake, M.J.<sup>1</sup>, Stewart, C.E.<sup>1</sup>, Erskine, R.M.<sup>1,3</sup>

5 <sup>1</sup>*Research Institute for Sport & Exercise Sciences, Liverpool John Moores University,*  
6 *Liverpool, United Kingdom.*

7 <sup>2</sup>*Exercise Biology Group, Faculty of Sport and Health Sciences, Technical University of Munich,*  
8 *Munich, Germany*

9 <sup>3</sup>*Institute of Sport, Exercise & Health, University College London, London, UK*

**Running title:** Neuromuscular Response following muscle damage *in vivo* and *in vitro*

**Address for reprint requests and all other correspondence:**

Philipp Baumert, Exercise Biology Group, Faculty of Sport and Health Sciences, Technical University of Munich, Munich, Germany; Email: philipp.baumert@tum.de

**Key words:** Exercise-induced muscle damage (EIMD); biceps femoris architecture; extracellular matrix (ECM); myoblast; fibroblast

**This is an original research article**

11 **ABSTRACT**

12 Hamstring muscle injury is highly prevalent in sports involving repeated maximal sprinting.  
13 Although neuromuscular fatigue is thought to be a risk factor, the mechanisms underlying the  
14 fatigue response to repeated maximal sprints are unclear. Here, we show that repeated  
15 maximal sprints induce neuromuscular fatigue accompanied with a prolonged strength loss in  
16 hamstring muscles. The immediate hamstring strength loss was linked to both central and  
17 peripheral fatigue, while prolonged strength loss was associated with indicators of muscle  
18 damage. The kinematic changes immediately after sprinting likely protected fatigued  
19 hamstrings from excess elongation stress, while larger hamstring muscle physiological cross-  
20 sectional area and lower *myoblast:fibroblast* ratio appeared to protect against fatigue/damage  
21 and improve muscle recovery within 48 h after sprinting. Contrastingly, a high  
22 *myoblast:fibroblast* ratio appears crucial for the latter stage of muscle regeneration. We have  
23 therefore identified novel mechanisms that likely regulate the fatigue/damage response and  
24 recovery following repeated maximal sprinting in humans.

25

26

27

28

29

30

## 31 INTRODUCTION

32 Hamstring strain is the most frequently occurring injury in sport (Crema *et al.*, 2017),  
33 particularly in those sports that involve high-speed running (Ekstrand *et al.*, 2011; Opar *et al.*,  
34 2012). Although the aetiology is unclear, numerous risk factors have been proposed, such as  
35 short fascicle length (Timmins *et al.*, 2015), poor flexibility (Jonhagen *et al.*, 1994), poor  
36 hamstring strength (Opar *et al.*, 2014), and inadequate warm-up (Woods *et al.*, 2007). Further,  
37 it is unknown whether hamstring strain is a result of a single event that exceeds the  
38 physiological range of hamstring muscle extensibility and contractility, or as a result of an  
39 accumulation of eccentric contractions during repeated maximal sprints, causing  
40 neuromuscular fatigue (Opar *et al.*, 2012). Neuromuscular fatigue is responsible for acute, as  
41 well as prolonged, impairment of muscle function and it can be classified as central fatigue  
42 (i.e. originating in the central nervous system), or as peripheral fatigue (i.e. distal to the  
43 neuromuscular junction) (Byrne *et al.*, 2004). Although it was recently reported that both central  
44 and peripheral fatigue contribute to impaired hamstring muscle function immediately after  
45 repeated maximal sprint-related interventions (Marshall *et al.*, 2014; Timmins *et al.*, 2014), the  
46 contribution of neuromuscular fatigue to hamstring muscle impairment and recovery over time  
47 is insufficiently studied following repeated maximal sprints (Verma *et al.*, 2015). An  
48 understanding of hamstring neuromuscular fatigue following repeated maximal sprints may be  
49 crucial for understanding hamstring strain aetiology (van der Horst *et al.*, 2015).

50 Peripheral fatigue may be caused by ultrastructural muscle damage, which is indicated by Z-  
51 line disturbance (Newham *et al.*, 1983) as well as disruption of the extracellular matrix (Stauber  
52 *et al.*, 1990). The extracellular matrix provides structural scaffolding for muscle remodelling  
53 and plays an integral role in force transmission (Wang *et al.*, 2009; Gillies & Lieber, 2011). This  
54 is referred to as exercise-induced muscle damage and it is exhibited by prolonged strength  
55 loss and delayed-onset muscle soreness, as well as the release of muscle-specific proteins  
56 [e.g. creatine kinase (CK)] into the circulation over the following days (Howatson & Van  
57 Someren, 2008). After substantial muscle damage, myogenic satellite cells (skeletal muscle

58 stem cells), play a key role in skeletal muscle regeneration and remodelling, as activated  
59 satellite cells (myoblasts) proliferate and migrate from their niche along the basal lamina to the  
60 injury site before terminally differentiating and fusing into myotubes (Tidball, 2011). There is  
61 increasing evidence that fibroblasts, the main cell type of muscle connective tissue, play a  
62 critical role in supporting muscle regeneration (Murphy *et al.*, 2011; Fry *et al.*, 2017; Mackey  
63 *et al.*, 2017). Following damage, infiltrating inflammatory cells activate muscle fibroblasts,  
64 which proliferate and migrate to the area of the myotrauma and produce extracellular matrix  
65 components in an orchestrated and regulated fashion to support healthy muscle remodelling  
66 (Joe *et al.*, 2010; Murphy *et al.*, 2011). However, less is known about the effect of fibroblasts  
67 on the initial response and recovery following *physiological* exercise-induced muscle damage,  
68 e.g. following repeated sprinting.

69 This acute damage to the muscle-tendon complex may facilitate hamstring strain, which is  
70 thought to occur in the late swing phase of sprinting, when the hamstring muscles contract  
71 eccentrically, i.e. trying to shorten while being lengthened in an attempt to decelerate the shaft  
72 before initial foot-ground contact (Thelen *et al.*, 2005; Chumanov *et al.*, 2012). Therefore, a  
73 short biceps femoris long head (BF<sub>LH</sub>) fascicle length has been suggested to increase  
74 hamstring strain risk (Timmins *et al.*, 2016a), as the BF<sub>LH</sub> is thought to be relatively more  
75 eccentrically stretched during the late swing phase of sprinting compared to the other  
76 hamstring muscles (Thelen *et al.*, 2005). However, no study has investigated the relationship  
77 between BF<sub>LH</sub> architecture (including muscle fascicle length and cross-sectional area), and the  
78 prolonged hamstring muscle response to exercise-induced neuromuscular fatigue. Finally,  
79 lower limb neuromuscular fatigue might cause a number of biomechanical alterations in  
80 running kinematics (Paschalis *et al.*, 2007). However, it is not known whether repeated  
81 maximal sprints influence kinematic patterns, and whether this can lead to prolonged changes  
82 in lower-limb kinematics, which may play a role in the development of muscle strain following  
83 insufficient recovery (Opar *et al.*, 2012).

84 Here we demonstrated that both central and peripheral fatigue contributed to the immediate  
85 loss of muscle function in both the quadriceps and hamstring muscle groups, but that  
86 peripheral factors mainly contributed to the sustained loss of hamstring muscle function.  
87 Moreover, we established that a lower myoblast:fibroblast ratio in isolated primary human  
88 muscle stem cells correlated with improved recovery from both repeated maximal sprints and  
89 an *in vitro* artificial wounding assay within the first 48 h. However, at seven days post damage,  
90 a higher myoblast:fibroblast ratio appears important for optimal muscle regeneration. We also  
91 found that BF<sub>LH</sub> architecture (i.e. PCSA) was associated with hamstring fatigue, and that  
92 neuromuscular fatigue led to reduced hip flexion and knee extension during the late swing  
93 phase of steady-state running. Thus, with this interdisciplinary study, we identify novel cellular  
94 and neuromuscular mechanisms underpinning central and peripheral fatigue following  
95 repeated sprinting, which ultimately led to kinematic changes during the running stride phase  
96 associated with hamstring strain injury.

97

## 98 **RESULTS**

### 99 **Effect of the Repeated Maximal Sprint Intervention on Neuromuscular Fatigue**

100 To begin examining the effect of repeated maximal sprints on neuromuscular fatigue, we  
101 measured different fatigue parameters before (PRE), immediately after (POST), and 48 h after  
102 (POST48) the repeated maximal sprint intervention. The average 30 m sprinting speed was  
103  $6.48 \pm 0.33 \text{ m s}^{-1}$ . There was a main effect of time for heart rate, 30 m sprinting time, rating of  
104 perceived exertion and lactate, with all parameters increasing from PRE to POST repeated  
105 maximal sprints (all  $P < 0.001$ ). Blood lactate concentration also increased from PRE ( $1.63 \pm$   
106  $0.45 \text{ mmol/L}$ ) to POST ( $9.82 \pm 3.62 \text{ mmol/L}$ ). The sprinting performance (measured via the  
107 performance decrement score (Glaister *et al.*, 2008)) decreased by  $3.98 \pm 2.99 \%$ , and rating  
108 of perceived exertion increased by  $96.5 \pm 35.2 \%$  from PRE-to-POST, indicating fatigue had  
109 occurred.

110 We then performed *in vivo* functional analysis to assess if repeated maximal sprints resulted  
 111 in an increase in central and/or peripheral fatigue. We, therefore, measured BF<sub>LH</sub> muscle  
 112 activation via normalised surface electromyography (sEMG) during hamstring maximum  
 113 voluntary contraction (MVC). That assessment showed that a change had occurred in sEMG  
 114 ( $F_{F2,24}=4.35$ ,  $P=0.022$ ), with post-hoc pairwise comparisons revealing a decrease from PRE-  
 115 to-POST ( $P=0.019$ ). However, this change was no longer evident at POST48 ( $P=0.157$ , Table  
 116 1), suggesting that central fatigue occurred immediately after repeated maximal sprints. No  
 117 other changes in muscle (co)activation were observed at any time point ( $P>0.05$ ).

118 **Table 1** Effect of the intermitted sprint intervention on measures of muscle activation. Data are  
 119 presented as mean  $\pm$  SD. One-way ANOVA, F- and P-values are reported.

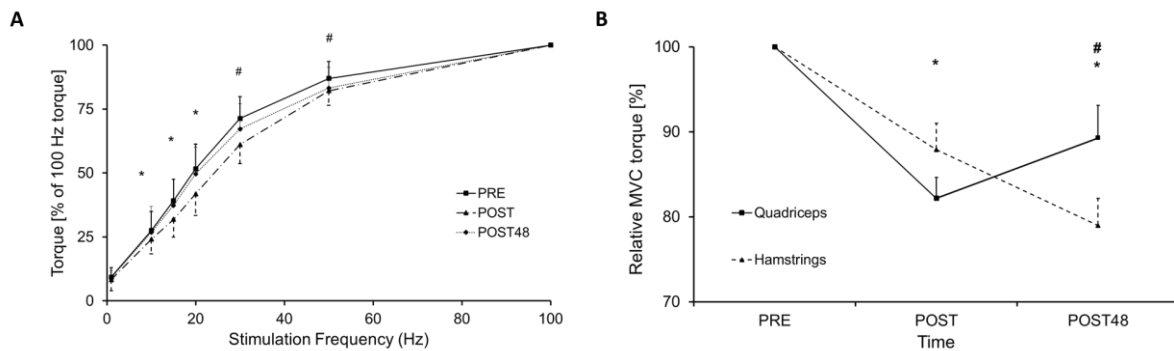
Assessment [unit]	n	PRE	POST	POST48	F-Test	P Value
Hamstring Muscle Voluntary Activation [ITT, %]	20	98.5 $\pm$ 2.64	94.1 $\pm$ 7.83	96.9 $\pm$ 5.96	F(1,4,38) = 2.75	0.099
Normalised BF <sub>LH</sub> knee flexion sEMG <sub>max</sub> [%]	14	3.32 $\pm$ 1.33	2.27 $\pm$ 0.72*	2.85 $\pm$ 1.16	F(2,24) = 4.35	0.022
Vastus lateralis knee extension sEMG <sub>max</sub> [mV]	15	0.50 $\pm$ 0.29	0.47 $\pm$ 0.34	0.51 $\pm$ 0.34	F(2,24) = 0.17	0.772
Quadriceps CoA during 30° hamstring MVC [%]	12	5.74 $\pm$ 7.23	4.08 $\pm$ 6.86	4.33 $\pm$ 8.76	F(2,22) = 0.50	0.613
Hamstring CoA during 80° quadriceps MVC [%]	10	4.79 $\pm$ 3.37	6.62 $\pm$ 3.79	7.51 $\pm$ 4.16	F(2,18) = 1.64	0.223

ITT – interpolated twitch technique; BF<sub>LH</sub> – Biceps femoris long head; CoA – Co-Activation; sEMG – surface Electromyography. \* Different to PRE ( $P<0.05$ ).

120  
 121 We also assessed the torque-frequency relationship *in vivo* via electrical stimulation, as it gives  
 122 an indication of peripheral (muscle) fatigue. There was an interaction between time x  
 123 stimulation frequency (n=19;  $F_{4,9,216}=6.62$ ,  $P<0.001$ ; Figure 1A). Post-hoc paired t-tests  
 124 revealed differences PRE-to-POST for 10-50 Hz, but lower frequencies between 10-20 Hz

125 reverted to baseline values POST48 ( $P>0.05$ ), while the frequencies of 30 and 50 Hz were still  
126 decreased POST48 compared to their baseline values ( $P<0.05$ ), providing evidence that  
127 peripheral fatigue occurred immediately after the repeated sprints and remained for 48 h

128



129

130 **Figure 1 (A)** Torque-frequency relationship, all frequencies were normalised to 100 Hz. \* significant  
131 differences between before (PRE) and immediately after (POST) the repeated maximal sprint  
132 intervention,  $P<0.05$ ; # significant differences between PRE and POST, and between PRE and POST48,  
133  $P<0.05$ . Data are presented as mean  $\pm$  SEM. **(B)** Comparison of relative maximal voluntary contraction  
134 (MVC) loss between hamstring and quadriceps muscle group before (PRE), immediately after (POST)  
135 and 48h after (POST48) the repeated maximal sprint intervention. \* significant differences compared to  
136 PRE,  $P<0.001$ ; # significant differences between quadriceps and hamstring MVC,  $P<0.05$ . Data are  
137 expressed as mean  $\pm$  SEM.

138

## 139 Effect of the Repeated Maximal Sprint Intervention on MVC Strength, Muscle 140 Soreness and Serum Markers of Exercise-Induced Muscle Damage

141 To investigate the effect of intermittent sprints on biomarkers of exercise-induced muscle  
142 damage, we assessed hamstring (knee flexion) and quadriceps (knee extension) MVC, muscle  
143 soreness, serum creatine kinase (CK) activity and interleukin-6 (IL-6) concentration PRE,  
144 POST and POST48. Isometric hamstring and quadriceps MVC, muscle soreness (all  $P<0.001$ )  
145 and serum CK activity ( $F_{1,3,34}=5.98$ ,  $P=0.017$ ), as well as IL-6 concentration ( $F_{1,3,34}=5.96$ ,  
146  $P=0.018$ ), showed a main effect of time, which are indicators of muscle damage (Table 2) that  
147 was similar to other studies (Howatson & Milak, 2009; Verma *et al.*, 2015; Chen *et al.*, 2017).  
148 Post-hoc pairwise comparisons revealed that, compared to PRE, both serum CK activity and  
149 serum IL-6 concentration were elevated at POST (both  $P=0.027$ ), and CK activity further

150 increased at POST48 ( $P=0.012$ ), while serum IL-6 concentration reverted to baseline values  
 151 ( $P>0.05$ ).

152 **Table 2** Effect of the Repeated Maximal Sprint Intervention on Muscle Damage-Biomarkers. Values  
 153 are mean  $\pm$  SD. One-way ANOVA, *F*- and *P*-values are reported.

Assessment [unit]	PRE	POST	POST48	F-Test	P Value
Quadriceps MVC [N·m]	270.5 $\pm$ 51.6*	222.4 $\pm$ 52.5*	243.0 $\pm$ 71.3*	F(2,38) = 16.55	<0.001
Hamstring MVC [N·m]	142.5 $\pm$ 25.0*	124.8 $\pm$ 29.9*	112.4 $\pm$ 30.1*	F(2,38) = 25.12	<0.001
Squat Muscle soreness [cm]	0.20 $\pm$ 0.41*	1.95 $\pm$ 1.61*	2.87 $\pm$ 1.71*	F(2,38) = 28.62	<0.001
Lunge Muscle soreness [cm]	0.30 $\pm$ 0.57	2.30 $\pm$ 2.08†	3.48 $\pm$ 2.07†	F(2,38) = 17.02	<0.001
Range of Motion [°]	120.3 $\pm$ 6.76	115.7 $\pm$ 6.77†	116.0 $\pm$ 6.27†	F(2,38) = 9.33	<0.001
CK activity [mU/mL]	27.9 $\pm$ 23.3	53.8 $\pm$ 45.3†	99.3 $\pm$ 104.5†	F(1,3,34) = 5.98	0.017
IL-6 concentration [pg/mL]	1.89 $\pm$ 3.10	7.68 $\pm$ 9.95#	1.59 $\pm$ 3.46	F(1,3,34) = 5.96	0.018

MVC – Maximal voluntary contraction; CK – Creatine Kinase; IL-6 – Interleukin-6; \* Significant differences between all time points; † differences PRE-to-POST and PRE-to-POST48 ( $P<0.05$ ); # differences PRE-to-POST and POST-to-POST48 ( $P<0.05$ ).

154 Further, there was an interaction between time and muscle groups concerning relative MVC  
 155 torque loss (percentage change from PRE MVC) ( $F_{1,4,38}=7.92$ ,  $P=0.004$ ). Relative MVC  
 156 decreased similarly in both quadriceps and hamstring muscle groups PRE-to-POST (Figure  
 157 1B). However, at POST48, hamstring MVC continued to decrease from POST ( $P=0.010$ ), while  
 158 quadriceps MVC began to return to PRE values ( $P=0.016$ ), and was higher than hamstring  
 159 MVC at POST48 ( $P=0.038$ ).



## 160 **Effect of the Repeated Maximal Sprint Intervention on Lower-Limb Kinematics**

161 To assess the consequential effect of neuromuscular fatigue on lower-limb kinematics, we  
162 captured treadmill running ( $4.17 \text{ m s}^{-1}$ ) kinematics with an eight-camera motion capture system  
163 over time. Three-dimensional motion analysis showed that there was a non-significant  
164 tendency for the duration of the running cycle to take longer POST and POST48, compared to  
165 PRE ( $P=0.080$ ; Table 3). Further, treadmill running demonstrated decreases in peak knee  
166 extension ( $P=0.047$ ) during the late swing phase at POST compared to PRE, but this reverted  
167 to baseline POST48. The percentage change in peak knee extension correlated with the  
168 percentage change in relative hamstring MVC torque both measured POST-to-POST48  
169 ( $r^2=0.258$ ,  $F_{1,2}=5.673$ ,  $P=0.031$ ).

**Table 3** Effect of the Repeated Maximal Sprint Intervention on Kinematics of Treadmill Running at 4.17 m s<sup>-1</sup>. Values are mean ± SD. One-way ANOVA, F- and P-values are reported.

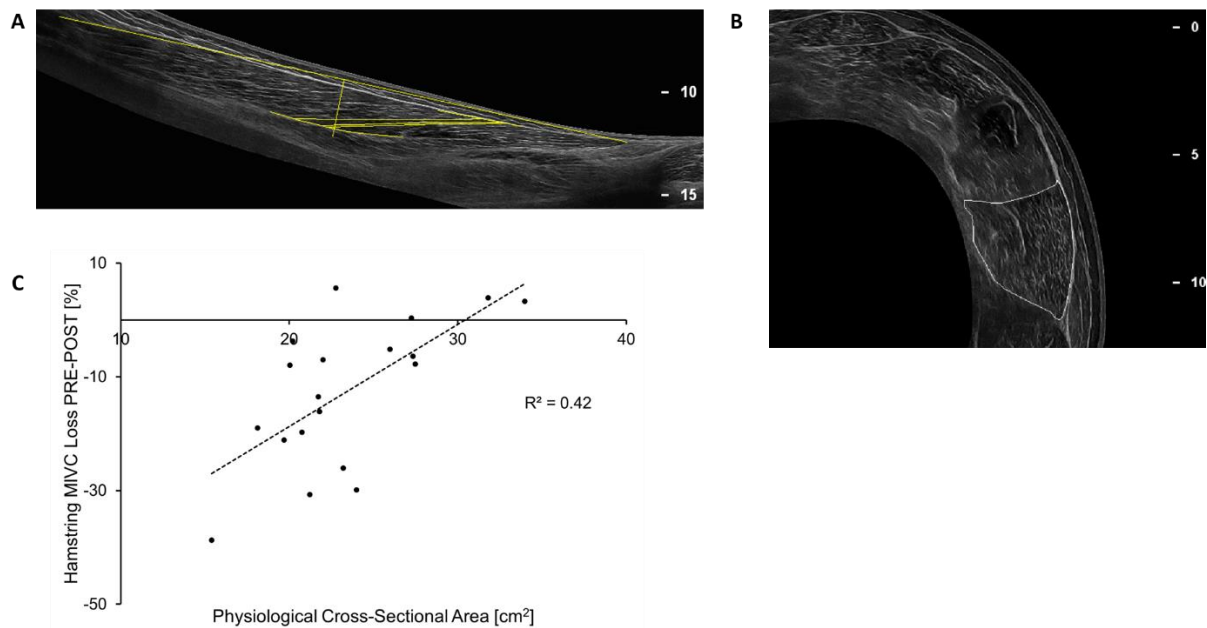
Kinematics [unit]	PRE	POST	POST48	F-Test	P Value
Peak knee flexion (swing phase) [°]	-103 ± 13.9	-110 ± 12.4	-108 ± 12.6	F(2,20) = 2.84	0.082
Peak knee extension (swing phase) [°]	-3.66 ± 5.32	-7.08 ± 5.07*	-4.29 ± 7.06	F(2,20) = 3.57	0.047
Contact hip flexion (toe strike) [°]	25.2 ± 5.42	29.3 ± 7.62	17.6 ± 15.6	F(1,2,20) = 4.05	0.062
Contact knee flexion (toe strike) [°]	-15.0 ± 6.25	-17.6 ± 6.79	-13.3 ± 9.64	F(2,22) = 2.79	0.083
Duration Running cycle [s]	0.67 ± 0.03	0.68 ± 0.03	0.69 ± 0.02	F(2,20) = 2.88	0.080
Stance phase duration [s]	0.18 ± 0.02	0.19 ± 0.02	0.19 ± 0.03	F(2,20) = 1.01	0.356
Swing Phase [s]	0.50 ± 0.04	0.50 ± 0.05	0.50 ± 0.03	F(1,2,20) = 0.03	0.899

Knee fully extended=0°; negative value indicates a flexed knee; \* different to PRE (P<0.05).

170

### 171 **Architecture of the Biceps Femoris Long Head Muscle**

172 To assess whether architectural parameters of the BF<sub>LH</sub> muscle (Figure 2A and B) were  
 173 associated with markers of peripheral fatigue, we performed ultrasound measurements of the  
 174 BF<sub>LH</sub> muscle (Table supplement 5). Muscle fascicle length and pennation angle of the BF<sub>LH</sub>,  
 175 which have previously been linked to hamstring muscle strain risk (Timmins *et al.*, 2016b), did  
 176 not correlate with any outcome variable of neuromuscular fatigue. However, BF<sub>LH</sub> PCSA (mean  
 177 ±SD: 23.4 ± 4.62 cm<sup>2</sup>) correlated inversely with relative hamstring MVC loss PRE-to-POST  
 178 (R<sup>2</sup>=0.421, F<sub>1,17</sub>=12.37, P=0.003, Figure 2C).



179

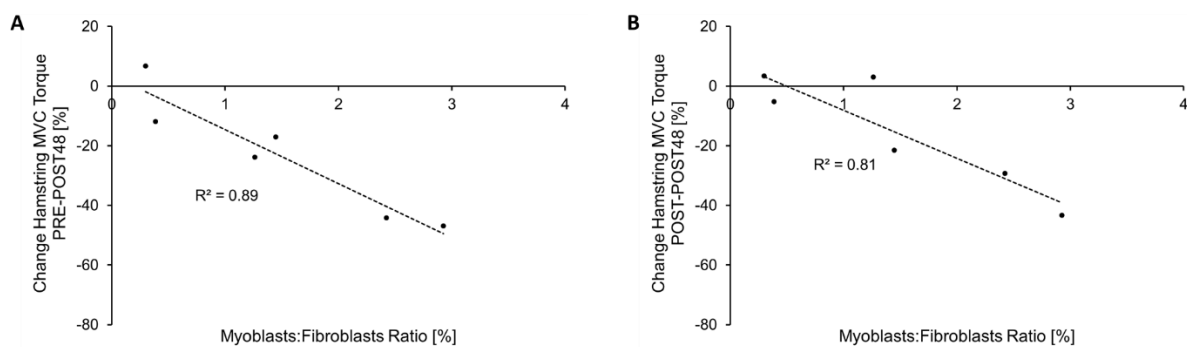
180 **Figure 2 (A)** Longitudinal image of biceps femoris long head, assessment of the biceps femoris long  
181 head is highlighted (total muscle length and fascicle length together with pennation angle at 50% of total  
182 muscle length). **(B)** Cross-sectional image at 60% muscle length (=100% proximal myotendinous  
183 junction), biceps femoris long head is highlighted. **(C)** Correlation between biceps femoris long head  
184 muscle physiological cross-sectional area and % hamstring maximum isometric voluntary contraction  
185 (MIVC) decrease from before (PRE) to immediately after (POST) the repeated maximal sprint  
186 intervention ( $P=0.003$ ).

187

## 188 **Comparison of the Muscle Response between the Repeated Maximal Sprint** 189 **Protocol and the Muscle Stem Cell Study**

190 We next sought to determine whether skeletal muscle stem cell composition (i.e.  
191 myoblast:fibroblast ratio) played a role in muscle strength recovery. Six of the 20 participants,  
192 who performed the repeated maximal sprint intervention, also volunteered to provide a muscle  
193 biopsy at least three weeks before the repeated maximal sprint intervention. As previous  
194 investigations have shown that skeletal muscles of different origin, but with similar  
195 physiological functions and fibre type composition, demonstrate similar transcriptome  
196 expression patterns of up to 99% (Evangelidis *et al.*, 2016; Terry *et al.*, 2018), we have taken  
197 a muscle biopsy from the vastus lateralis as a representative muscle of the quadriceps and  
198 hamstring muscle groups. The muscle stem cells were isolated, cultured and then  
199 characterized by immunofluorescence staining. The mean  $\pm$  SD myoblast:fibroblast ratio of the  
200 six participants was  $1.46 \pm 1.06$  (range: 0.299 to 2.93). There was a strong inverse correlation

201 between myoblast:fibroblast ratio and the percentage change in relative hamstring MVC torque  
202 measured PRE-to-POST48 *in vivo* ( $R=-0.945$ ,  $F_{1,4}=33.73$ ,  $P=0.004$ ; Figure 3A). Thus, the  
203 myoblast:fibroblast ratio explained 89% of the variability in strength recovery PRE-to-POST48,  
204 i.e. participants with a high myoblast:fibroblast ratio showed a delayed hamstring strength  
205 recovery 48 h after repeated maximal sprints compared to those with a low myoblast:fibroblast  
206 ratio. Further, there was an inverse correlation between myoblast:fibroblast ratio and relative  
207 hamstring MVC torque measured POST-to-POST48 ( $R=-0.943$ ,  $F_{1,4}=17.08$ ,  $P=0.014$ ; Figure  
208 3B). Thus, the myoblast:fibroblast ratio explained 81% of the variability in strength recovery  
209 POST-to-POST48. No correlations were found between the myoblast:fibroblast ratio and  
210 changes in quadriceps MVC torque or with any other muscle damage and fatigue biomarker  
211 following repeated maximal sprints.



212

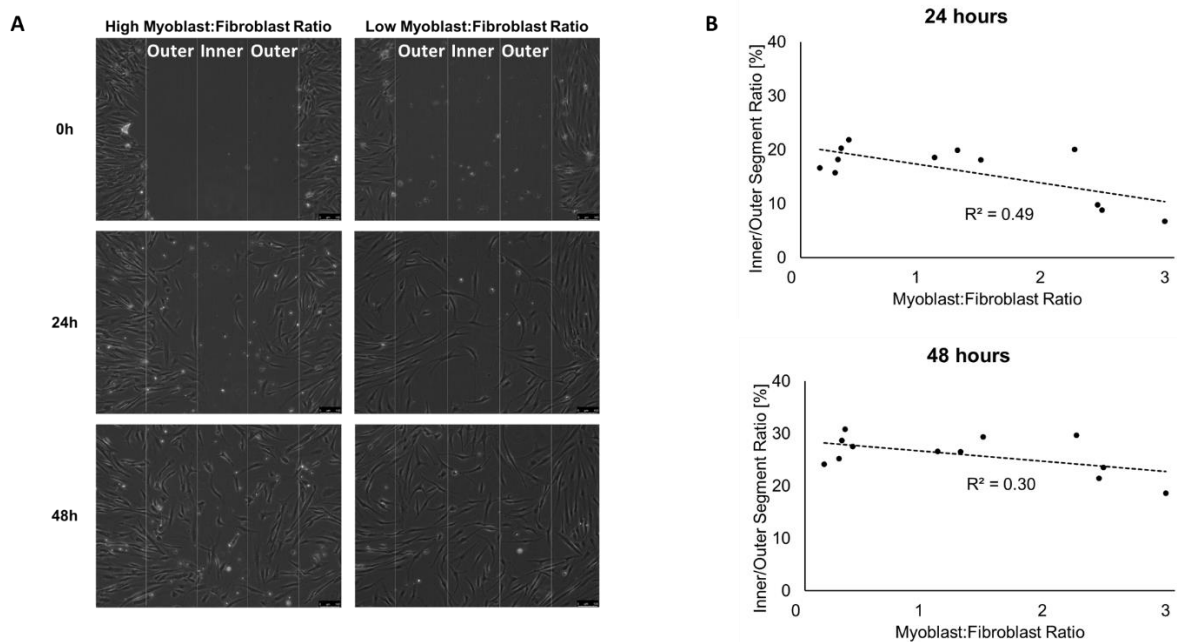
213 **Figure 3** Inverse correlation between the myoblast:fibroblast ratio, assessed in the current *in vitro* study  
214 and the change of hamstring MVC torque measured (A) before and 48 h after ( $P=0.004$ ), and (B)  
215 measured immediately after and 48 h after ( $P=0.014$ ) (B) the repeated maximal sprint intervention.

216

## 217 Artificial Wound Healing Assay to Investigate Repair and Regeneration 218 Regarding Myoblast:Fibroblast Ratio

219 To further assess the effect of the myoblast:fibroblast ratio on skeletal muscle recovery, we  
220 performed an *in vitro* artificial wounding (scratch) assay. We used primary human skeletal  
221 muscle stem cells derived from the six volunteers, who participated in both the repeated  
222 maximal sprint intervention and volunteered to provide a muscle biopsy, and another six (two  
223 male and four females), who did not participate in the repeated maximal sprint intervention (to

224 increase the power of the *in vitro* study). We did not detect any differences in muscle stem cell  
225 characteristics between cells obtained from females and males (data not shown). We,  
226 therefore, combined the data from all muscle cells and correlated the muscle characteristics  
227 with individual myoblast:fibroblast ratios. We observed no correlations regarding  
228 myoblast:fibroblast ratio and the total number of myoblasts and fibroblasts migrating into the  
229 artificial wound within all three segments combined at 24 h ( $R^2=0.20$ ,  $F_{1,10}=2.56$ ,  $P=0.141$ ) or  
230 48 h ( $R^2=0.02$ ,  $F_{1,10}=0.19$ ,  $P=0.671$ ) after the scratch assay.



231

232 **Figure 4 (A)** Representative images for cell migration of muscle cells with a high myoblast:fibroblast  
233 ratio (2.4; left) and with a low percentage of myoblasts (0.3; right) into the artificial wound. The wound  
234 area is about 900  $\mu\text{m}$  in width and split into 3 x 300  $\mu\text{m}$  segments (one inner and two outer segments).  
235 Magnification is x 10.5, and scale bar is 100  $\mu\text{m}$ . **(B)** Inverse correlations between the myoblast:fibroblast  
236 ratio and the migration dynamics of 12 different primary muscle stem cells 24 h ( $P=0.011$ ) and a trend  
237 48 h ( $P=0.064$ ) after the artificial wound healing assay.

238 However, there was an inverse correlation between myoblast:fibroblast ratio and migration  
239 dynamics for the 12 participants (Figure 4 B). Muscle stem cells with a low myoblast:fibroblast  
240 ratio demonstrated more cells in the inner segment than to the outer segment compared to  
241 muscle stem cells with high myoblast:fibroblast ratio at 24 h ( $R^2=0.49$ ,  $F_{1,10}=9.53$ ,  $P=0.011$ )  
242 and with a non-significant trend at 48 h ( $R^2=0.30$ ,  $F_{1,10}=4.33$ ,  $P=0.064$ ) after the artificial wound  
243 healing assay. Further, there were positive correlations between the myoblast:fibroblast ratio  
244 and all parameters at seven and 10 days after the artificial wound healing assay (all  $P<0.05$ ;

245 Table supplement 6). Biopsies with a higher myoblast:fibroblast ratio showed more myotubes  
246 per field, which had a higher diameter and area compared to biopsies with a lower  
247 myoblast:fibroblast ratio (Figure supplement 5).

248

## 249 **DISCUSSION**

250 In this study, we have used an interdisciplinary approach to systematically investigate the  
251 biomechanical, physiological and cellular factors underpinning neuromuscular fatigue following  
252 repeated maximal sprints. We have shown that immediate strength loss was associated with  
253 reduced hamstring sEMG activity (indicating impaired hamstring motor unit recruitment) and  
254 markers of peripheral fatigue, but the magnitude and sustained changes in MVC torque over  
255 time (especially of the hamstrings) was largely associated with indicators of peripheral fatigue.  
256 Muscle damage biomarkers indicated that the peripheral fatigue might have been caused  
257 predominantly by ultrastructural damage within the hamstring muscle tissue. Further, both  
258 central and peripheral fatigue caused by repeated maximal sprints appeared to affect the  
259 neuromuscular control of running patterns and  $BF_{LH}$  PCSA correlated inversely with the change  
260 in hamstring MVC torque immediately after the repeated maximal sprint intervention. A high  
261 myoblast:fibroblast ratio showed a delayed wound closure *in vitro* and a delayed MVC torque  
262 recovery following repeated maximal sprints *in vivo* within the first 48 h, indicating that stem  
263 cells of the non-contractile muscle tissue might positively affect the response to muscle  
264 damaging exercises. However, a higher myoblast:fibroblast ratio led to better myotube  
265 formation at seven days, and higher CK activity at ten days, after the scratch assay, suggesting  
266 that myoblasts are important for the latter stage of muscle regeneration.

### 267 **Fatigue and Muscle Damage Following Repeated Maximal Sprints**

268 We showed a decreased activity of normalised  $BF_{LH}$  sEMG activity immediately after the  
269 repeated maximal sprint intervention, but no significant changes in neuromuscular activation  
270 using the interpolated twitch technique. The discrepancy between these two methods might

271 be explained by the fact that voluntary activation measured via the interpolated twitch  
272 technique investigates all of the hamstring muscles, whilst the normalised EMG analysis was  
273 confined solely to the BF<sub>LH</sub>, which is in line with a previous study (Marshall *et al.*, 2014). We  
274 assume that BF<sub>LH</sub> might fatigue to a greater degree immediately after repeated maximal sprint  
275 related interventions compared to the other hamstring muscles. However, we also provide  
276 evidence for peripheral fatigue occurring immediately after the repeated maximal sprints, and  
277 a delayed recovery at higher frequencies (30-50 Hz) after observing a right shift in the torque-  
278 frequency relationship. This may be due to ultrastructural damage predominantly in fast-twitch  
279 (which fire at rates from 30-50 Hz) compared to slow-twitch muscle fibres (discharge rates 10-  
280 25 Hz) (Friden *et al.*, 1983; Jones *et al.*, 1986), leading to impaired force generation rather  
281 than simply fatiguing the muscle fibres.

282 Both the quadriceps and hamstring muscle groups showed similar strength loss immediately  
283 after the repeated maximal sprints, but the hamstring muscle group showed further strength  
284 loss 48 h later compared to the quadriceps. Other studies did not show this additional strength  
285 loss for the hamstring muscle group POST48. Differences in the training status of the  
286 participants (Verma *et al.*, 2015; Chen *et al.*, 2017) and in the methodological approaches  
287 (Balsom *et al.*, 1992) might partly explain the different outcomes. The peak BF<sub>LH</sub> EMG activity  
288 occurs at a more extended knee angle during hamstring isokinetic muscle contraction  
289 compared to the peak EMG occurring at a more flexed knee angle for the other hamstring  
290 muscles, such as the semitendinosus (Onishi *et al.*, 2002). Therefore, we suggest that the BF<sub>LH</sub>  
291 is the key hamstring muscle responsible for decelerating the shaft at the end of the late swing  
292 phase. After repeated bouts of high-speed running, the semitendinosus might fatigue  
293 prematurely (Schuermans *et al.*, 2014) and the BF<sub>LH</sub> would need to substitute the impaired  
294 function of the preceding semitendinosus to decelerate the shaft.

## 295 **Kinematic Analysis**

296 Our *in vivo* intervention caused changes in the running kinematics with reduced knee extension  
297 in the late swing phase immediately after the repeated maximal sprints. Reduced hamstring

298 muscle strength due to neuromuscular fatigue might trigger a protective mechanism directly  
299 after repeated maximal sprints. Afferent signals from the fatigued and damaged hamstrings  
300 might activate the Golgi tendon organ (Byrne *et al.*, 2004), thus limiting hamstring muscle fibre  
301 strain in an attempt to minimise further muscle damage. These kinematic changes were not  
302 evident 48 h after the repeated maximal sprints. However, there was a non-significant tendency  
303 for prolonged stride duration during running ( $P = 0.08$ , data not shown) 48 h later and the  
304 percentage change of knee extension in the late swing phase of running correlated with  
305 changes in hamstring strength both measured from POST to POST48. This indicates that  
306 participants with delayed hamstring strength recovery were still not able to fully control running.  
307 As hamstring MVC continued to deteriorate 48 h after intermittent sprints but quadriceps MVC  
308 started to improve, it could be that lower-limb kinematics in the sagittal plane are controlled by  
309 the hamstrings more than the quadriceps. Ultrastructural damage in the hamstring muscles  
310 might lead to decelerated movement patterns over time, which could increase the risk for  
311 hamstring strain injury during sprinting (Opar *et al.*, 2012).

## 312 **The Role of the Extracellular Matrix on the Muscle Response Following Repeated** 313 **maximal sprinting**

314 Recent investigations have suggested that hamstring maximum eccentric strength and  $BF_{LH}$   
315 fascicle length are predictors of hamstring strain injury (Timmins *et al.*, 2016a). Further, a  
316 fatigued muscle is likely to accentuate the risk of muscle strain (Ekstrand *et al.*, 2011). However,  
317 we could not find any correlation between  $BF_{LH}$  fascicle length and any biomarker of fatigue  
318 but  $BF_{LH}$  PCSA correlated inversely with hamstring strength loss from PRE to POST. During  
319 the late swing phase of sprinting, the hamstring muscles contract eccentrically to  
320 decelerate the shaft and to enhance the subsequent concentric shortening contraction for  
321 maximal sprinting by using stored elastic energy from the muscle-tendon unit. In comparison  
322 to other conventional muscle-damaging interventions (Franchi & Maffiuletti, 2019), this  
323 dynamic (stretch-shortening) movements might lead to an additional damage of the hamstring  
324 muscle connective tissue structure. Therefore, a larger  $BF_{LH}$  PCSA might protect against



325 immediate hamstring MVC loss due to a greater ability to transmit the ground reaction forces  
326 laterally (from fibre to fibre) (Turrina *et al.*, 2013), which might disperse the force more  
327 efficiently to the tendon, while the muscle fibres themselves undergo less strain. Further, a  
328 greater BF<sub>LH</sub> PCSA reflects more fibres aligned in parallel, which would be accompanied by  
329 more muscle connective tissue of the extracellular matrix, thus potentially protecting the  
330 muscle fibres from excessive damage during eccentric contractions.

331 The stem cells of the extracellular matrix also demonstrated an important role for muscle  
332 strength recovery in the subgroup of participants, as there was a strong inverse correlation  
333 between myoblast:fibroblast ratio and hamstring MVC torque recovery POST48. Skeletal  
334 muscles with an increased availability of fibroblasts around the area of myotrauma might have  
335 a better capacity to reorganise the complex extracellular matrix, thus restoring (lateral) force  
336 transmission, which results in a faster recovery of muscle strength after muscle damage. This  
337 was in line with the myoblast:fibroblast ratio effect on cellular aspects of muscle regeneration  
338 and remodelling assessed in primary muscle stem cells *in vitro*. Muscle stem cells with a low  
339 myoblast:fibroblast ratio revealed a faster wound closure (i.e. more cells migrated to the inner  
340 part of the artificial injury compared to the outer part), in particular 24 h after performing the  
341 scratch assay. However, this effect was less significant 48 h after the scratch protocol, and, at  
342 day seven, muscle primary cells with a higher myoblast:fibroblast ratio showed an improved  
343 myotube formation, which is in line with the investigation of Fry *et al.* (2014). Together, these  
344 results suggest that the abundance and activity of fibroblasts and myoblasts may play different  
345 roles, depending on the time points during muscle repair. A larger abundance of fibroblasts  
346 has a positive effect at the beginning of muscle repair, but a larger number of myoblasts is  
347 more important for the latter stage of muscle regeneration or hypertrophy, when myoblasts  
348 differentiate and fuse to become myotubes. We, therefore, assume that repeated maximal  
349 sprints with insufficient recovery of previously fatigued and damage muscles (where the fatigue  
350 and damage response is modulated by the muscle size and stem cell composition, respectively)  
351 might augment the risk of muscle strains, as appropriate damage to the muscle connective

352 tissue is thought to differentiate between exercise-induced muscle damage and muscle strains  
353 (Valle *et al.*, 2017; Balius *et al.*, 2018).

## 354 **Limitations**

355 There was no relationship between the myoblast:fibroblast ratio and any physiological  
356 variables regarding the quadriceps femoris, from which the muscle biopsies were obtained. It  
357 has previously been shown that skeletal muscles of different origin, but with similar  
358 physiological functions and fibre type composition, demonstrate similar transcriptome  
359 expression patterns of up to 99% (Evangelidis *et al.*, 2016; Terry *et al.*, 2018). Therefore, the  
360 correlation between myoblast:fibroblast ratio and the muscle damage-response of the  
361 hamstrings but not the quadriceps muscles is likely explained by more severe ultrastructural  
362 damage in the hamstrings than quadriceps. Furthermore, peripheral fatigue can be caused by  
363 metabolic perturbations, such as the depletion of intramuscular glycogen (Howatson & Van  
364 Someren, 2008). Therefore, because we did not control diet throughout the study, it is possible  
365 that inter-individual differences in baseline muscle glycogen may have influenced the ability to  
366 maintain maximal intensity throughout the sprints. However, participants were instructed to eat  
367 and drink similar foods two hours before each laboratory visit, and to avoid strenuous exercise  
368 for at least 48 h prior to the testing. Further, participants were given sufficient recovery between  
369 sprint repetitions and there was a low decrement in sprint performance, indicating that  
370 glycogen depletion was probably only a minor factor.

## 371 **CONCLUSION**

372 Repeated maximal sprints induces a greater and more prolonged strength loss in the  
373 hamstrings compared to the quadriceps muscles. The immediate loss of hamstring function  
374 appears to be due to both central (particularly reduced neuromuscular activation of the biceps  
375 femoris long head) and peripheral fatigue, while prolonged hamstring strength loss is  
376 predominantly linked to peripheral fatigue. Thigh neuromuscular fatigue following repeated  
377 maximal sprints alters hip and knee kinematics during running immediately after the repeated

378 maximal sprints, but this (likely) protective effect is less evident 48 hours after the intervention,  
379 which may lead to an increased hamstring muscle injury risk. Furthermore, biceps femoris long  
380 head PCSA was inversely related to hamstring strength loss immediately after repeated  
381 maximal sprinting, suggesting that the structure of the muscle, including non-contractile tissue  
382 (e.g. the extracellular matrix) protects against neuromuscular fatigue. Skeletal muscles with an  
383 increased number of fibroblasts might have a better capacity to reorganise the complex  
384 extracellular matrix, which results in a faster recovery of muscle function after substantial  
385 muscle damage. However, a larger number of myoblasts seems to be more important for the  
386 latter stage of muscle regeneration. These novel findings improve our understanding of the  
387 physiological, biomechanical and cellular causes and effects of exercise-induced  
388 neuromuscular fatigue. The practical implications are that a 48 h recovery period following  
389 repeated maximal sprinting is insufficient, and might increase hamstring strain injury risk.  
390 Furthermore, increasing hamstring PCSA via resistance training is likely to reduce peripheral  
391 fatigue following repeated maximal sprinting, thereby reducing hamstring strain injury risk.

## 392 MATERIALS AND METHODS

### 393 Participants

394 *In vivo repeated maximal sprint intervention:* Twenty recreationally active and healthy young  
395 men (*mean*  $\pm$  *SD*; age  $20.3 \pm 2.87$  years; height  $1.79 \pm 0.05$  m; body mass  $75.0 \pm 7.89$  kg)  
396 participated in the repeated maximal sprint intervention.

397 *In vitro muscle stem cell component:* Eight healthy young male (age  $21.25 \pm 4.27$  years; height  
398  $1.77 \pm 0.05$  m; body mass  $73.78 \pm 5.68$  kg) and four healthy young female (age  $25.5 \pm 1.29$   
399 years; height  $1.67 \pm 0.08$  m; body mass  $61.40 \pm 2.57$  kg) participants provided a biopsy of  
400 the vastus lateralis muscle for the *in vitro* muscle stem cell component of this study. Six of the  
401 eight males also participated in the repeated maximal sprint intervention at least three weeks  
402 after providing a muscle biopsy. Only males were recruited for the repeated maximal sprint  
403 intervention, as there is some evidence of sex differences in neuromuscular fatigue (Wüst *et*  
404 *al.*, 2008). However, both men and women were recruited for the muscle stem cell component  
405 due to there being no reported sex differences in stem cell properties and none within our own  
406 pilot studies (data not shown). Prior to starting the study, written informed consent was  
407 obtained from each participant and pre-biopsy screening was performed by a physician for  
408 those participants who volunteered a muscle biopsy. The study was approved by the Research  
409 Ethics Committee of Liverpool John Moores University and complied with the Declaration of  
410 Helsinki. Volunteers were physically active but were ineligible to participate if they had  
411 performed strength training of the lower limbs within 6 months prior to participation in the study,  
412 which was determined during pre-participation screening. Further exclusion criteria were: (i)  
413 any lower limb injury in the past 12 months; (ii) age under 18 or above 35 years; and (iii) more  
414 than three structured exercise sessions per week.

### 415 Experimental Design of the Repeated Maximal Sprint Intervention *in vivo*

416 Participants were required to visit the temperature-controlled ( $22\text{-}24^{\circ}\text{C}$ ) laboratory on three  
417 occasions: (i) familiarisation, (ii) testing day including the PRE and POST assessments; and

418 (iii) POST48 assessments after the repeated maximal sprint intervention. One week prior to  
419 the testing day, participants were familiarised with the assessments as well as with repeated  
420 maximal sprints (by performing 2-3 submaximal sprints) and BF<sub>LH</sub> architecture of the hamstring  
421 muscle group was assessed via ultrasound. On the test day, participants performed the  
422 repeated maximal sprint intervention of 15 x 30 m sprints to induce neuromuscular  
423 fatigue/damage in both the quadriceps femoris and hamstring muscle groups. All tests were  
424 performed at the same time of the day for each participant. Further, participants were instructed  
425 to maintain their normal routine (including eating habits), to refrain from drinking alcohol and  
426 to avoid any strenuous exercise 48 h prior to testing and throughout the study, and to refrain  
427 from consuming caffeine on testing days. Nothing was consumed throughout the testing  
428 sessions except water, which was available ad libitum.

429 The test battery was always performed in the same order with the right leg of each participant  
430 and comprised (i) venous blood sampling [for analysing serum interleukin-6 (IL-6)  
431 concentration and creatine kinase (CK) activity]; (ii) hamstrings and quadriceps muscle  
432 soreness via visual analogue scale; (iii) isometric maximum voluntary contraction (MVC)  
433 torque of the quadriceps, as well as both voluntary and involuntary muscle activation and  
434 torque-frequency relationship via electrical stimulation] MVC torque of the hamstring together  
435 with normalised BF<sub>LH</sub> sEMG (see below); and (iv) treadmill running ( $4.17 \text{ m s}^{-1}$ ) kinematics of  
436 the right leg (via an eight-camera motion capture system) PRE and POST48 following the  
437 repeated maximal sprint intervention. At POST, kinematic assessments were performed first  
438 followed by the aforementioned order of the assessment for practical reasons.

### 439 **Maximal Repeated Sprint Protocol**

440 Many athletes in team sports are required to perform repeated maximal sprints, which are  
441 characterised by short-duration (<10 s) and relatively longer recovery times (>60 s) between  
442 maximal sprint bouts, and have a different physiological demand compared to repeated-sprint  
443 exercises with shorter recovery times (<60 s) (Bradley *et al.*, 2010; Girard *et al.*, 2011).  
444 Therefore, the IS intervention consisted of 15 repetitions of 30 m maximal sprints with a

445 deceleration zone of 12 m. The 30 m distance was chosen as the upper average of both the  
446 total sprinting distance ( $346 \pm 115$  m) of wide-midfielders and the mean recovery time ( $70.2 \pm$   
447  $25.1$  s) between sprint bouts in soccer (Bradley *et al.*, 2009; Bradley *et al.*, 2010), which allows  
448 the athlete to maintain the performance of the sprint bouts. Similar protocols have been used  
449 elsewhere (Timmins *et al.*, 2014; Verma *et al.*, 2015; Chen *et al.*, 2017). Prior to the repeated  
450 maximal sprint intervention, a five-minute warm-up was performed, comprising jogging,  
451 dynamic stretching and three self-paced 20 m runs at 60%, 80%, 100% of perceived top speed.  
452 During the repeated maximal sprint intervention, the participants were instructed to sprint  
453 maximally (verbal encouragement) and to stop within the deceleration zone. Further, they were  
454 instructed to move slowly back to the start line and to sit on a chair for the remaining time until  
455 the next sprint. The recovery comprised 90 s between repetitions and after every 5<sup>th</sup> repetition,  
456 the participants were allowed to rest for 3 min. Sprinting time during trials was measured and  
457 controlled with timing gates (Brower Timing Systems, Draper, UT, USA), which were placed  
458 on the start and finish line. Participants started 30 cm before the start line to avoid interfering  
459 with timing gates with the arms upon initial acceleration (Howatson & Milak, 2009). Further,  
460 heart rate (Polar Oy, Kempele, Finland) and rating of perceived exertion (Borg, 1982) were  
461 recorded before and after each repetition. Participants were instructed to wear the same  
462 footwear for each testing day. As there was an upsurge in speed of the final sprint, fatigue was  
463 assessed with the performance decrement score using the following formula (Glaister *et al.*,  
464 2008):

$$465 \quad \textit{Fatigue} = (100 \times (\textit{total sprint time} \div \textit{ideal sprint time})) - 100$$

466 Where total sprint time = sum of time from all 15 sprints; and ideal sprint time = total number  
467 of sprints (15) x fastest repetition sprint time. The calculation of this decrement score was also  
468 used to quantify changes in heart rate and rating of perceived exertion during the repeated  
469 maximal sprint intervention.

## 470 **Maximal Voluntary Contraction (MVC)**

471 Three test sessions were conducted with an isokinetic dynamometer (Humac Norm, CSMI  
472 Solutions, Massachusetts, USA). As *isokinetic* maximum voluntary contractions (MVC) torque  
473 tests are only weak predictors of hamstring strain injury (van Dyk *et al.*, 2016), we decided to  
474 focus on *isometric* MVC quadriceps and hamstring torque at optimal knee strength angles  
475 (optimal torque-joint angle relationship, see below) to avoid further fatiguing the participants.  
476 The torque signal was interfaced with an acquisition system (AcqKnowledge, Biopac Systems,  
477 Santa Barbara, USA) for analogue-to-digital conversion and sampled at a frequency of 2 kHz.  
478 The participant was seated in an upright position and securely fastened with inextensible straps  
479 at the chest and waist while the arms were held crossed above the chest. The tibiofemoral  
480 epicondyle was aligned with the lever arm rotation axis, and the lever arm shin pad was  
481 strapped to the leg, 2 cm above the centre of the lateral malleolus. A Velcro strap secured the  
482 distal thigh just above the knee. The hip joint angle was set to 85° (180° = supine position) in  
483 order to analyse the knee flexor muscle group at a sprint specific angle associated with the  
484 late swing phase of sprinting (Guex *et al.*, 2012). Participants were instructed to maximally  
485 extend and flex their leg to measure knee range of motion. Quadriceps MVC was measured  
486 at 80° knee flexion (0° = full knee extension), as this is the optimal joint angle for peak  
487 quadriceps MVC in healthy young men (Erskine *et al.*, 2009). Hamstring MVC was measured  
488 at 30° knee flexion based on this being the optimal joint angle for peak hamstring MVC during  
489 our pilot work. Published studies during the time of data collection used a similar angle of  
490 hamstring MVC torque (Nedelec *et al.*, 2014; Kirk & Rice, 2016). This was also in line with  
491 sprinting kinematics, demonstrating that maximal hamstring muscle lengths during sprinting  
492 occur during the late swing phase when the knee is flexed between 30° and 45° (Thelen *et al.*,  
493 2005). Prior to isometric MVC assessments, participants underwent a standardised warm up  
494 consisting of 10 submaximal isokinetic leg extensions (60°·s<sup>-1</sup>). Participants then performed  
495 three isometric knee extension (quadriceps) and flexion (hamstring) at both joint angles (each  
496 MVC lasting 2-3 s), with 60 s rest between MVC of a given muscle group. The highest MVC of

497 the three attempts for each muscle group at each angle was used for subsequent analyses.  
498 Throughout the tests, participants received verbal encouragement and biofeedback (MVC  
499 outputs) were projected onto a screen in front of the participant.

## 500 **Hamstring Muscle Voluntary Activation**

501 To measure hamstring muscle voluntary activation capacity via the interpolated twitch  
502 technique, stimulation electrodes (12.5 mm x 7.5 mm self-adhesive electrodes (DJO Global,  
503 California, USA) were used. The general procedure has been described elsewhere (Erskine  
504 *et al.*, 2009; Erskine *et al.*, 2010; Marshall *et al.*, 2014). Briefly, the anode was placed proximal  
505 to the popliteal fossa, and the cathode was placed beneath the gluteal fold and slightly medial  
506 to avoid activation of the vastus lateralis. Protocols were completed with electrical stimulation  
507 pads carefully taped down during the sprinting protocol and were additionally marked on the  
508 skin with a permanent marker, to ensure a precise relocation for the POST and POST48 tests.  
509 Stimulation was delivered by a high-voltage stimulator (DS7AH; Digitimer Ltd., Welwyn Garden  
510 City, United Kingdom), and consisted of a doublet using two 240-V rectangular pulses (200  $\mu$ s  
511 pulse width) with an inter-pulse duration of 10 ms (100 Hz stimulation). During each  
512 experimental session, relaxed hamstring muscles were stimulated while participants were fixed  
513 in the isokinetic dynamometer with the same setting for knee flexion MVC (85° hip angle, 30 °  
514 knee flexion). The amplitude started with 50 mA to familiarise the participants to the stimulation  
515 and was gradually increased in 20 mA increments until a plateau in doublet torque was  
516 achieved. We decided to use the individual maximal stimulation (100 %) intensity despite the  
517 fact that other publications used supramaximal stimulation (110-130 %) (Marshall *et al.*, 2014)  
518 as we experienced lower MVC knee flexion torque output beyond 100 %. That individual  
519 amplitude (162.0  $\pm$  17.4 mA; range: 130–200 mA) was applied during all maximal contractions  
520 in the experimental session.

521 The maximal doublet stimulation was used two minutes later to elicit resting maximal doublet  
522 torque in the resting state (control doublet), followed 2.5 s later by a second (superimposed)  
523 doublet during an isometric knee flexion MVC. The superimposed doublet torque was always



524 calculated manually from careful selection and inspection of the respective time periods  
525 compared to a normal increase in voluntary torque. Voluntary activation was calculated  
526 according to the following equation:

$$527 \quad VA (\%) = [1 - (\textit{superimposed doublet torque} / \textit{control doublet torque})]$$

## 528 **Surface Electromyography and Antagonist Muscle Co-activation**

529 Surface electromyographic (sEMG) activity was recorded from the vastus lateralis and BF<sub>LH</sub> to  
530 determine the extent of antagonist muscle co-activation during MVCs of the respective muscle  
531 group. Previous reports have shown that the vastus lateralis (Reeves *et al.*, 2004) and BF<sub>LH</sub>  
532 (Kellis & Baltzopoulos, 1999) are representative muscles for the quadriceps femoris and  
533 hamstring muscle group, respectively. This procedure has been reported in detail elsewhere  
534 (Reeves *et al.*, 2004). Briefly, once the muscles were identified via palpation, and the skin  
535 surface was shaved and cleaned with 70% ethanol, two bipolar Ag-AgCl surface electrodes  
536 with an inter-electrode distance of 2 cm (Noraxon duel sEMG electrode, Noraxon, Scottsdale,  
537 USA) were placed along the sagittal axis over the muscle belly at 33% of the respective muscle  
538 length from the distal end [according to SENIAM guidelines (Hermens *et al.*, 2000)] and one  
539 reference electrode (Ambu Blue, Ambu, Copenhagen, Denmark) was positioned over the  
540 medial tibial condyle. The exact location of the electrodes were marked on the participant's  
541 skin with a permanent marker to ensure precise electrode repositioning for the following  
542 assessments.

543 Surface EMG signals were sampled at 2000 Hz (Biopac Systems, Santa Barbara, USA) and  
544 then band-pass filtered between 10–500 Hz (AcqKnowledge, Biopac Systems, Santa Barbara,  
545 USA). Surface EMG activity of both the agonist and antagonist muscles were analysed by  
546 calculating the root mean square of the sEMG signal of a 500-ms epoch around peak MVC.  
547 To compare BF<sub>LH</sub> sEMG activity at all three time points, BF<sub>LH</sub> sEMG of the hamstring MVC at  
548 30° was normalised to the evoked maximum compound muscle action potential (M-wave) of  
549 the BF<sub>LH</sub> (see below). Antagonist muscle co-activation (i.e. quadriceps activation during

550 hamstring MVC at 30° knee flexion, or hamstring activation during quadriceps MVC at 80°  
551 knee flexion) was calculated with the following formula (where  $EMG_{max}$  is the maximum sEMG  
552 of the antagonist muscle when acting as an agonist at the same knee joint angle):

$$553 \quad \textit{Antagonist muscle co - activation} = \frac{EMG_{antagonist}}{EMG_{max}} \times 100$$

554 Torque signals, electrical stimuli, and sEMG activity were displayed on a computer screen,  
555 interfaced with an acquisition system (AcqKnowledge, Biopac Systems, Santa Barbara, USA)  
556 used for analogue-to-digital conversion. Due to technical issues, co-activation data were  
557 available for hamstring  $n = 12$ ; and quadriceps  $n=10$ .

### 558 **Hamstring Muscle Maximal Compound Muscle Action Potential**

559 The hamstring muscle group was stimulated with single square wave twitch pulses (200  $\mu$ s  
560 duration) using the same electrical stimulator and stimulating electrodes, as described above.  
561 While the participant sat resting on the isokinetic dynamometer with the knee angle set at 30°  
562 knee flexion, compound muscle action potentials ( $M$ -waves) were evoked with 10 to 20 mA  
563 incremental amplitudes until a maximal  $M$ -wave ( $M_{max}$ ) was achieved. The average amplitude  
564 necessary to evoke a maximal  $M$ -wave was  $166.8 \pm 19.8$  mA; range: 130–210 mA). The  
565 maximal  $M$ -wave was defined as the mean peak-to-peak sEMG response from the three  
566 highest observed  $M$ -waves. Due to inter-individual differences in subcutaneous fat and the  
567 (re)location of small sEMG electrodes over a relatively large muscle belly, sEMG amplitude is  
568 notoriously variable (Araujo *et al.*, 2000). To reduce this inter- and intra-individual variability,  
569 we normalised absolute  $BF_{LH}$  sEMG to the individual's  $BF_{LH}$  maximal  $M$ -wave, determined at  
570 each testing session (Lanza *et al.*, 2018). Due to technical issues, data of  $BF_{LH}$  sEMG  
571 normalised to maximal  $M$ -wave was only available for  $n = 13$ .

### 572 **Torque-frequency Relationship**

573 The torque-frequency relationship was determined by stimulating the hamstring muscle group  
574 with single square wave twitch pulses (200  $\mu$ s duration) at 1, 10, 15, 20, 30, 50 and 100 Hz for

575 1 s each in a random order and with 15 s rest between each stimulation, using the same  
576 electrical stimulator and stimulating electrodes (and location), as described above. The  
577 stimulus intensity for 100-Hz stimulation was the amplitude necessary to elicit ~20 % knee  
578 flexion MVC torque at PRE, and the same amplitude was used for the same test at POST and  
579 48POST. The absolute peak torque at each frequency was normalised to the peak torque at  
580 100 Hz for each time point (PRE, POST and POST48).

### 581 **Delayed Onset Muscle Soreness**

582 Using a visual analogue scale that consisted of a 100 mm line (scale 0-10 cm; 0 cm=no  
583 soreness; 10 cm= unbearably painful), in conjunction with both a three-repetition bilateral squat  
584 (predominantly to determine quadriceps femoris muscle soreness) (Scott & Huskisson, 1979)  
585 and lunges (predominantly to determine hamstring muscle soreness), participants rated their  
586 perceived lower limb muscle soreness along the muscle length immediately after each  
587 movement. Muscle soreness was also measured by recording the force required to elicit  
588 tenderness at nine fixed sites on the skin over the quadriceps (distal, central and proximal  
589 locations of the three superficial quadriceps heads, vastus lateralis, vastus medialis and rectus  
590 femoris) and six sites on the hamstrings (distal, central and proximal locations of both BF<sub>LH</sub>  
591 and the medial hamstrings), which were previously marked with a permanent marker to ensure  
592 the same measuring position PRE, POST and POST48. At each site, a gradually increasing  
593 force was applied by the investigator with an algometer (FPK/FPN Mechanical Algometer,  
594 Wagner Instruments, Greenwich, USA) with a maximum of 10 kg/cm<sup>2</sup>. Lying in the prone  
595 position with the hip and knee fully extended and muscles relaxed, the participant was asked  
596 to indicate when the sensation of pressure changed to discomfort, and the force at that point  
597 was recorded (Newham *et al.*, 1987).

### 598 **Ultrasound**

599 Architectural parameters of the BF<sub>LH</sub> were assessed using B-mode ultrasound imaging.  
600 Participants were in the prone position with the hip and knee fully extended and muscles

601 relaxed. The BF<sub>LH</sub> was investigated, as this muscle is the most commonly injured hamstring  
602 muscle in team sports, particularly during sprinting (Ekstrand *et al.*, 2011). Longitudinal and  
603 cross-sectional panoramic ultrasound images of the right BF<sub>LH</sub> were obtained (Philips EPIQ 7  
604 Ultrasound System, Bothel, USA). The linear transducer (5-18 MHz; aperture 38.9 mm) was  
605 carefully placed on the skin with transmission gel and BF<sub>LH</sub> was scanned (i) longitudinally from  
606 its distal (=0% muscle length) to proximal (=100% muscle length) myotendinous junction along  
607 a line drawn with a permanent marker to mark the central pathway between the medial and  
608 lateral aspects of the muscle (incorporating the intra-muscular aponeurosis (Evangelidis *et al.*,  
609 2014) (Figure 2A); and (ii) cross-sectionally at 20, 40, 60 and 80% along the total muscle length,  
610 measured on the skin using a tape measure (Seca, Hamburg, Germany) (Figure 2B).

611 All images were analysed offline (ImageJ, version 1.51s, National Institutes of Health,  
612 Bethesda, USA). Two images for each of the four cross-sectional points were recorded and  
613 the image of best quality was used to calculate BF<sub>LH</sub> muscle volume. The volume of the  
614 muscular portion between every two consecutive scans was calculated with the following  
615 equation:

$$616 \quad \text{Volume} = \frac{1}{3} * d * \left( a + \sqrt{(ab) + b} \right)$$

617 Where *a* and *b* are the anatomical cross-sectional areas of the muscle of two consecutive  
618 cross-sectional scans and *d* is the interval distance between the cross-sectional area  
619 measurements. The volume of the entire muscle was calculated by summing up all of the inter-  
620 scan muscular volumes (Erskine *et al.*, 2016). Two full-length sagittal images were then  
621 recorded to allow for the measurement of resting BF<sub>LH</sub> muscle fascicle length and pennation  
622 angle, which were both assessed in 3 fascicles at 50 % of the total length of BF<sub>LH</sub>. This point  
623 was measured offline (ImageJ). A comparison between offline (sagittal ultrasound) and tape  
624 measurements of the total BF<sub>LH</sub> length revealed a very high correlation ( $R^2=0.958$ ,  $P<0.001$ ).  
625 Fascicle length was measured by tracing the fascicular path from the upper aponeurosis to the  
626 intra-muscular aponeurosis of the BF<sub>LH</sub>. Muscle fascicle pennation angle was determined as

627 the angle between the muscle fascicular paths and their insertion into the intra-muscular  
628 aponeurosis. The mean of the three measurements for each parameter were used to  
629 determine both fascicle length and pennation angle of the BF<sub>LH</sub> muscle. PCSA was calculated  
630 by dividing BF<sub>LH</sub> volume by its fascicle length. During the time of data collection, a similar  
631 methodological approach was published elsewhere (Seymore *et al.*, 2017). One longitudinal  
632 image of one participant in the present study was not analysed due to low image quality.  
633 Ultrasound scans and image analysis was performed by the same investigator.

### 634 **Kinematic and Kinetic Data**

635 Three-dimensional kinematic and kinetic data were synchronously collected at 500 Hz using  
636 an eight-camera motion analysis system (Qqus 300+; Qualisys, Gothenburg, Sweden),  
637 together with a ground-embedded force plate (90 x 60 cm, 9287B; Kistler Holding, Winterthur,  
638 Switzerland) at 1,500 Hz. The data were filtered with a digital dual low-pass Butterworth filter  
639 at 20 Hz for motion and 60 Hz for force, as previously described (Verheul *et al.*, 2017).  
640 Retroreflective markers (12 mm diameter) were placed on anatomical landmarks on the right  
641 leg and pelvis, as previously described (McClay & Manal, 1999). One standing static and two  
642 functional motion calibration trials were recorded of the participant PRE, POST and POST48.  
643 For the static trial, participants stood with their feet approximately shoulder width apart and  
644 knees fully extended. This static trial determined local coordinate systems, the location of joint  
645 centres, and the foot, shank, thigh, and pelvis segment lengths of each participant. The  
646 functional trials defined functional hip joint centres (Schwartz & Rozumalski, 2005) and knee  
647 joint axes (Robinson & Vanrenterghem, 2012). Kinematic data were tracked using Qualisys  
648 Track Manager Software (Qualisys). Data processing and analysis were undertaken in  
649 Visual3D (C-Motion, Germantown, MD). To examine any changes between the time points,  
650 joint angles were normalised relative to the static trial of the accompanying time point for  
651 minimising the influence of potential slightly different marker positions between the trials.  
652 Lower extremity 3D joint angles and angular velocities were calculated using an X-Y-Z Cardan  
653 angle rotation sequence. Investigated variables included peak knee and hip angles, as well as

654 range of motion and time during stance and swing phase of the treadmill run, for all three  
655 planes, were calculated as described in previous studies (Verheul *et al.*, 2017).

### 656 **Motorised Treadmill Run**

657 Participants ran on a motorised treadmill (HP Cosmos Pulsar; Nussdorf, Germany) for 30 s at  
658 4.17 m s<sup>-1</sup> (0° incline), as high-speed running was of interest. The selected speed was based  
659 on pilot testing, which demonstrated that 15 km/h was the fastest speed on a motorized  
660 treadmill where the participants still felt comfortable. Motion analysis data were recorded for  
661 the last 10 s of the run and data were analysed for at least 6 consecutive strides. Peak knee  
662 and hip angle data, for all three planes, were calculated (i) between the initial contact and  
663 terminal stance of foot; and (ii) between initial and terminal swing phase. The touchdown of  
664 the foot during the treadmill run was determined from the kinematic data as occurring at the  
665 local minima and the toe-off during running as the local maxima of the vertical velocity of the  
666 head of the fifth metatarsal marker on the foot (Maiwald *et al.*, 2009).

### 667 **Blood Samples**

668 A 10 mL blood sample was drawn from an antecubital vein in the forearm and collected into a  
669 serum vacutainer (BD Vacutainer systems, Plymouth, UK). The blood samples were obtained  
670 at each time point and left at 22-24°C for 30 min to allow clotting, and then kept on ice when  
671 necessary. Serum samples were centrifuged at 1,300 g for 15 min at 4°C. All samples were  
672 then aliquoted into 1.5 mL microcentrifuge tubes [Axygen (Corning), New York, USA] and  
673 stored at -80°C until subsequent analysis (see below).

### 674 **Serum Interleukin-6 (IL-6) Concentration**

675 Serum samples were assayed for IL-6 concentration using commercially available human IL-  
676 6 enzyme linked immunosorbent assay kits (Quantikine®, R&D systems, Minneapolis, MN,  
677 USA) according to the manufacturer's instructions. The intensity of the colour produced after  
678 20 min was measured with a Thermo Multiskan Spectrum microplate reader (Thermo Fisher

679 Scientific. Waltham, MA. USA) at 450 nm and values were calculated with Excel 365 (Microsoft,  
680 v. 365, USA) by generating a four-parameter logistic curve fit. The minimum detectable dose  
681 of human IL-6 was 0.70 pg/mL.

### 682 **Serum Creatine Kinase Activity**

683 Creatine kinase (CK) activity was assayed using a commercially available CK assay  
684 (Catachem Inc., Connecticut, NE, USA), as described in detail elsewhere (Owens *et al.*, 2015).  
685 Briefly, 10  $\mu$ L blood serum were loaded onto a 96-well UV plate. The CK reaction reagent and  
686 diluent (Catachem) were prepared as per the manufacturer's instructions and added to the  
687 samples and the change in absorbance monitored continuously over 20 min in a Thermo  
688 Multiskan Spectrum plate reader (Thermo Fisher Scientific. Waltham, MA. USA) at a  
689 wavelength of 340 nm.

### 690 **Capillary Blood Lactate Concentration**

691 Capillary blood samples were taken from the finger-tip via a Safety-Lancet Extra 18G needle  
692 (Sarstedt; Nümbrecht, Germany) at rest before and immediately after the repeated maximal  
693 sprint intervention. Blood samples were analysed within 60 seconds of collection using a  
694 portable blood lactate analyser (Arkay Lactate Pro; Kyoto, Japan).

### 695 **Reagents, Chemicals, and Solvents for Muscle Cell Culture *in vitro***

696 Growth media used for the expansion of human muscle-derived cell populations consisted of  
697 Hams F-10 nutrient mix (Lonza, Basel, Switzerland) with added L-glutamine (2.5 mM), 10%  
698 heat-inactivated fetal bovine serum (hiFBS; Gibco, Thermo Fisher Scientific, Altincham, UK),  
699 1% penicillin-streptomycin (Life Technologies, Warrington, UK), and 1% L-Glutamine (Gibco).  
700 Differentiation media consisted of  $\alpha$ -MEM (Lonza), 1% hiFBS, 1% penicillin-streptomycin, and  
701 1% L-glutamine. Phosphate-buffered saline (PBS; Sigma-Aldrich) was used to wash cell  
702 monolayers. Desmin polyclonal rabbit anti-human antibody (Cat# ab15200, RRID: AB\_301744)  
703 was used (1:200) from Abcam (Abcam, Cambridge, UK), and secondary antibody (TRITC

704 polyclonal goat anti-rabbit; Cat# A16101, RRID: AB\_2534775) was used (1:200) from Fisher  
705 Scientific.

## 706 **Muscle Biopsy Procedure**

707 Participants were instructed to avoid any strenuous exercise 48 h prior to the biopsy procedure.  
708 Biopsies from the vastus lateralis muscle were obtained under local anaesthesia from each  
709 participant, using the Weil-Blakesley conchotome technique as described previously  
710 (Baczynska *et al.*, 2016). The conchotome was inserted through the incision into the muscle  
711 belly to obtain the  $134 \pm 82.7$  mg muscle biopsy.

## 712 **Extraction of Human Muscle-Derived Cells**

713 The muscle biopsies analysed in this study were isolated (Blau & Webster, 1981; Crown *et al.*,  
714 2000) and cultured (Owens *et al.*, 2015), as reported previously. Briefly, biopsy samples were  
715 transferred with precooled growth media from the muscle biopsy suite to the sterile tissue  
716 culture hood (Kojair Biowizard Silverline class II hood; Kojair, Vippula, Finland) within 40 min  
717 and muscle biopsy samples were washed three times with ice-cold PBS (0.01 M phosphate  
718 buffer, 0.0027 M KCl, and 0.137 M NaCl, pH 7.4, in dH<sub>2</sub>O). Visible fibrous and fat tissue was  
719 removed using sterile scissor and forceps. Samples were cut in small pieces (1 mm<sup>3</sup>) and  
720 digested in 5 ml of trypsin-EDTA for 15 min on a magnetic stirring platform at 37°C to dissociate  
721 muscle cells. The trypsinisation process was repeated twice. Supernatant derived following  
722 each treatment was collected and pooled with hiFBS at a concentration of 10% of the total  
723 volume to inhibit further protease activity. Cell supernatant was centrifuged at 450 g for 5 min.  
724 Supernatant was discarded and the cell pellet was resuspended in growth media and plated  
725 on a T25 cm<sup>2</sup> culture flask (Corning, Life Sciences, New York, USA) for cell population  
726 expansion. Culture flasks were previously coated with a 2 mg/l porcine gelatin solution (90–  
727 110 g, Bloom; Sigma-Aldrich, Dorset, UK) to support cell adhesion.



## 728 **Expansion of Extracted Cells**

729 The medium was refreshed on the fourth day after the extraction procedure and subsequently  
730 every 48 h following two brief washes with PBS. Cells were incubated in a HERAcell 150i CO<sub>2</sub>  
731 Incubator (Thermo Scientific, Cheshire, UK). T25 cm<sup>2</sup> culture flasks reached 80% confluence  
732 after approximately 10 days and were passaged via trypsinisation. Cells were counted using  
733 Trypan Blue exclusion and re-plated on gelatinised T75 cm<sup>2</sup> culture flasks (Nunc, Roskilde,  
734 Denmark). The cells were expanded until passage 3 and then frozen in GM with 10% dimethyl  
735 sulfoxide (DMSO) in liquid N<sub>2</sub> as a cryopreservant. All experiments were performed on cells  
736 between passages 3 and 6 to avoid potential issues of senescence (Foulstone *et al.*, 2004).

## 737 **Characterization of Human Muscle-Derived Cells**

738 The mixed population of human skeletal muscle-derived myoblasts and fibroblasts were  
739 characterised by immunofluorescent staining for the detection of desmin expressed by  
740 myoblasts (desmin positive) and non-myoblasts (desmin negative) to determine the  
741 percentage of myoblasts and fibroblasts. Previous investigations have determined that the  
742 non-myoblast (desmin negative) fraction is highly enriched in fibroblasts, with up to 99 % of  
743 this fraction being fibroblasts (Stewart *et al.*, 2003; Agle *et al.*, 2013). Therefore, non-  
744 myoblasts (desmin negative) were referred to here as fibroblasts.

745 Grohmann *et al.* (2005) showed that passaging does not change the percentage of myoblast  
746 and fibroblasts and all populations were included for analysis. Monolayers were incubated with  
747 25% [vol/vol methanol in Tris-buffered saline (10 mM Tris-HCl, pH 7.8, 150 mM NaCl)], 50%  
748 and 100% for 5-min to fix the cells and stored at 4°C wet in Tris-buffered saline until further  
749 analysis. Fixed monolayers were permeabilised and blocked for 2 h with 5% goat serum and  
750 0.2% Triton X-100 in Tris-buffered saline, prior to staining. Cells were incubated overnight at  
751 4°C with anti-Desmin antibody (1:200). After overnight incubation, the primary antibody was  
752 removed, and the cells were washed three times with Tris-buffered saline. Secondary TRITC  
753 polyclonal goat anti-rabbit antibody (1:200) was then applied and incubated for 2 h at 4°C.

754 Fluorescent images were captured using live imaging microscopy (Leica DMB 6000;  
755 Magnification x 10.5) and analysed via ImageJ cell counter plug-in. A total of four randomly  
756 selected areas per well were analysed per individual.

## 757 **Wound-Healing Assay, Migration and Differentiation Analysis**

758 For the wound healing assay, 100,000 cells/ml were seeded in gelatinised six-well plates (Nunc,  
759 Roskilde, Denmark). Cells were expanded as described above until cell monolayers reached  
760 a confluent state, Growth media was removed, monolayers were washed with PBS and cells  
761 were damaged by a vertical scrape with a 1-ml pipette tip (width of the wound area, *mean* ±  
762 *S.E.M.*: 896.4 ± 21.24 µm), as previously reported by our group (Owens *et al.*, 2015; Brown *et*  
763 *al.*, 2017). PBS was aspirated, damaged cell monolayers were washed twice with PBS to  
764 remove cell debris and 2 ml differentiation media was added. Monolayers were imaged with a  
765 live imaging microscopy (Leica) for the analysis of cell migration immediately, 24h, 48h and  
766 seven days after the wound healing assay. Additional 500 µl differentiation media was added  
767 in each well at day 4. TIF images were exported from Leica Application Suite and loaded as  
768 TIF image stacks in ImageJ with a cell counter plug-in. Cells in the outer and inner segments  
769 were then counted (Figure 4A).

770 Damaged monolayers were imaged at two sites per well in the wound site immediately post-  
771 damage (0 h). These image coordinates were tracked and stored to allow subsequent  
772 monitoring of the same sites on the wound to reduce this experimental bias. Myotube formation  
773 was captured on day 7. Captured images were exported as TIF image files, and analysed in  
774 ImageJ. Muscle cell fusion/differentiation was assessed as the number of myotubes per field  
775 of view and myotube hypertrophy was determined by measuring myotube length, myotube  
776 diameter (the average of three diameters along the length of the myotube), myotube area  
777 (determined by manually drawing a line around the sarcolemma of each myotube) and total  
778 myotube number via ImageJ cell counter plug-in. By normalising the pixel scale to the micron  
779 scale of each image, a value expressed as µm<sup>2</sup> was obtained for myotube area. A total of two  
780 images per well were analysed.

## 781 **Creatine Kinase (CK) Activity**

782 At 0 and 10 days following the mechanical scrape insult, CK activity was analysed as a marker  
783 of muscle cell differentiation/fusion into myotubes. Cell monolayers were first lysed with 300  
784  $\mu$ l/well of 50 M Tris-mes and 1% Triton-X 100, pH 7.8 (TMT). Ten microliters of TMT cell lysate  
785 was loaded in duplicate wells on a 96-well UV plate and used for quantification of CK activity.  
786 The CK reaction reagent and diluent (Catachem, Bridgeport, CT, USA) were prepared as per  
787 the manufacturer's instructions as previously described (please see subsection Serum  
788 Creatine Kinase).

## 789 **Statistical Analysis**

790 One-way repeated-measures analysis of variances (ANOVA)s were performed to determine  
791 whether there was a significant main effect for time (within subject factor) for the following  
792 dependent variables: MVC torque, voluntary muscle activation, antagonist muscle co-  
793 activation, muscle soreness (for squat lunge via measured via visual analogue scale as well  
794 as algometer), rating of perceived exertion, CK activity, IL-6 concentration, and for kinematics  
795 data (hip and knee angle parameters). MVC torque data were analysed for interactions and  
796 main effects for muscle group and time using two-way mixed design ANOVAs, comparing  
797 differences between muscle groups across 3-time points; PRE, POST, and POST48. For  
798 within test comparisons, either, independent t-tests, or one-way ANOVAs were used where  
799 appropriate. For the torque-frequency relationship, normalised torque at each frequency was  
800 analysed using a two-way repeated measures ANOVA, with stimulation frequency (1-100 Hz)  
801 and time (PRE, POST and POST48) as the within-groups independent variables. Post-hoc  
802 one-way repeated measures ANOVAs were used to determine if the normalised torque at each  
803 frequency differed between time points. Bivariate correlations were used to analyse the relation  
804 between architectural parameters of the BF<sub>LH</sub> (volume, fascicle length, fascicle pennation angle  
805 and PCSA) and fatigue biomarkers (relative MVC loss normalised to PRE MVC), serum CK  
806 activity, serum IL-6 concentration, muscle soreness, knee joint range of motion or changes in  
807 range of motion during treadmill running.

808 Bivariate correlations were used to analyse the relation between myoblast:fibroblast ratio and  
809 quadriceps and hamstring MVC, migration dynamics (total cell migration, cell proportion of  
810 inner to outer segment) and myotube formation (total myotube number, myotube length,  
811 average diameter, myotube area and CK activity) of the muscle stem cells. Standard guidelines  
812 concerning violation of the sphericity assumption to adjust the degree of freedom of the F-test  
813 by the Huynh-Feldt epsilon if epsilon is greater than 0.75 and to use the more stringent  
814 Greenhouse-Geisser adjustment if epsilon is less than 0.75 were followed. Results were  
815 expressed as mean  $\pm$  SD, unless otherwise stated, with statistical significance set at  $P < 0.05$ .  
816 All MVC data were analysed with AcqKnowledge software 4.4 (Biopac-Systems Inc., Goleta,  
817 USA) and SPSS 23 Software (IBM Inc., Armonk, NY: IBM Corp) was used for statistical  
818 analysis. Occasional missing data are reflected in the reported degrees of freedom.

## 819 **GRANTS**

820 This study was supported by a Liverpool John Moores University PhD studentship (P.B.) and  
821 the Wellcome Trust Biomedical Vacation Scholarships (R.M.E., M.S.).

## 822 **DISCLOSURES**

823 No conflicts of interest, financial or otherwise, are declared by the authors.

## 824 **AUTHOR CONTRIBUTION**

825 R.M.E, P.B., B.D., C.E.S., and M.L. conceived and designed the research; P.B., S.T., M.S.,  
826 M.C., J.A.S., and S.O.S performed the experiments; P.B., S.T. and R.M.E analyzed the data;  
827 R.M.E., P.B, M.L. and C.E.S. interpreted the results of the experiments; P.B. prepared the  
828 figures; P.B. drafted the manuscript; R.M.E., P.B., S.T., M.S., M.L., B.D., C.E.S., M.C., J.A.S.,  
829 and S.O.S edited and approved the final version of the manuscript.

830

## 831 **REFERENCES**

832 Agle CC, Rowler AM, Velloso CP, Lazarus NR & Harridge SD. (2013). Human skeletal muscle  
833 fibroblasts, but not myogenic cells, readily undergo adipogenic differentiation. *Journal of cell*  
834 *science, jcs*. 132563.

835

- 836 Araujo RC, Duarte M & Amadio AC. (2000). On the inter-and intra-subject variability of the  
837 electromyographic signal in isometric contractions. *Electromyogr Clin Neurophysiol* **40**, 225-  
838 230.  
839
- 840 Baczynska AM, Shaw S, Roberts HC, Cooper C, Sayer AA & Patel HP. (2016). Human Vastus Lateralis  
841 Skeletal Muscle Biopsy Using the Weil-Blakesley Conchotome. *Journal of Visualized*  
842 *Experiments*, e53075-e53075.  
843
- 844 Balius R, Alomar X, Pedret C, Blasi M, Rodas G, Pruna R, Peña-Amaro J & Fernández-Jaén T. (2018).  
845 Role of the Extracellular Matrix in Muscle Injuries: Histoarchitectural Considerations for  
846 Muscle Injuries. *Orthopaedic Journal of Sports Medicine* **6**, 2325967118795863.  
847
- 848 Balsom P, Seger J, Sjödin B & Ekblom B. (1992). Maximal-intensity intermittent exercise: effect of  
849 recovery duration. *Int J Sports Med* **13**, 528-528.  
850
- 851 Blau HM & Webster C. (1981). Isolation and characterization of human muscle cells. *Proc Natl Acad*  
852 *Sci* **78**, 5623-5627.  
853
- 854 Borg GA. (1982). Psychophysical bases of perceived exertion. *Medicine and science in sports and*  
855 *exercise* **14**, 377-381.  
856
- 857 Bradley PS, Di Mascio M, Peart D, Olsen P & Sheldon B. (2010). High-intensity activity profiles of elite  
858 soccer players at different performance levels. *J Strength Cond* **24**, 2343-2351.  
859
- 860 Bradley PS, Sheldon W, Wooster B, Olsen P, Boanas P & Krstrup P. (2009). High-intensity running in  
861 English FA Premier League soccer matches. *Journal of sports sciences* **27**, 159-168.  
862
- 863 Brown AD, Close GL, Sharples AP & Stewart CE. (2017). Murine myoblast migration: influence of  
864 replicative ageing and nutrition. *Biogerontology* **18**, 947-964.  
865
- 866 Byrne C, Twist C & Eston R. (2004). Neuromuscular function after exercise-induced muscle damage.  
867 *Sports Med* **34**, 49-69.  
868
- 869 Chen C-H, Ye X, Wang Y-T, Chen Y-S & Tseng W-C. (2017). Differential Effects of Different Warm-up  
870 Protocols on Repeated Sprints-Induced Muscle Damage. *J Strength Cond*.  
871
- 872 Chumanov ES, Schache AG, Heiderscheit BC & Thelen DG. (2012). Hamstrings are most susceptible to  
873 injury during the late swing phase of sprinting. *Br J Sports Med* **46**, 90.  
874
- 875 Crema MD, Jarraya M, Engebretsen L, Roemer FW, Hayashi D, Domingues R, Skaf AY & Guermazi A.  
876 (2017). Imaging-detected acute muscle injuries in athletes participating in the Rio de Janeiro  
877 2016 Summer Olympic Games. *Br J Sports Med*, bjsports-2017-098247.  
878
- 879 Crown A, He X, Holly J, Lightman S & Stewart C. (2000). Characterisation of the IGF system in a  
880 primary adult human skeletal muscle cell model, and comparison of the effects of insulin and  
881 IGF-I on protein metabolism. *J Endocrinol* **167**, 403-415.  
882
- 883 Ekstrand J, Hägglund M & Waldén M. (2011). Epidemiology of muscle injuries in professional football  
884 (soccer). *The American journal of sports medicine* **39**, 1226-1232.  
885

- 886 Erskine R, Tomlinson D, Morse C, Winwood K, Hampson P, Lord J & Onambélé G. (2016). The  
887 individual and combined effects of obesity-and ageing-induced systemic inflammation on  
888 human skeletal muscle properties. *Int J Obes (Lond)*.  
889
- 890 Erskine RM, Jones DA, Maganaris CN & Degens H. (2009). In vivo specific tension of the human  
891 quadriceps femoris muscle. *Eur J Appl Physiol* **106**, 827-838.  
892
- 893 Erskine RM, Jones DA, Williams AG, Stewart CE & Degens H. (2010). Resistance training increases in  
894 vivo quadriceps femoris muscle specific tension in young men. *Acta physiologica* **199**, 83-89.  
895
- 896 Evangelidis P, Massey GJ, Ferguson RA, Wheeler PC, Pain MT & Folland JP. (2016). The functional  
897 significance of hamstrings composition: is it really a 'fast' muscle group? *Scandinavian journal*  
898 *of medicine & science in sports* **27**, 1181-1189.  
899
- 900 Evangelidis PE, Massey GJ, Pain M & Folland JP. (2014). Biceps Femoris Aponeurosis Size: A Potential  
901 Risk Factor for Strain Injury? *Medicine and science in sports and exercise*.  
902
- 903 Foulstone EJ, Huser C, Crown AL, Holly JM & Stewart CE. (2004). Differential signalling mechanisms  
904 predisposing primary human skeletal muscle cells to altered proliferation and differentiation:  
905 roles of IGF-I and TNF $\alpha$ . *Experimental cell research* **294**, 223-235.  
906
- 907 Franchi MV & Maffiuletti NA. (2019). Distinct modalities of eccentric exercise: different recipes, not  
908 the same dish. *J Appl Physiol* **0**, null.  
909
- 910 Friden J, Sjöström M & Ekblom B. (1983). Myofibrillar damage following intense eccentric exercise in  
911 man. *Int J Sports Med* **4**, 170-176.  
912
- 913 Fry CS, Kirby TJ, Kosmac K, McCarthy JJ & Peterson CA. (2017). Myogenic progenitor cells control  
914 extracellular matrix production by fibroblasts during skeletal muscle hypertrophy. *Cell stem*  
915 *cell* **20**, 56-69.  
916
- 917 Fry CS, Lee JD, Jackson JR, Kirby TJ, Stasko SA, Liu H, Dupont-Versteegden EE, McCarthy JJ & Peterson  
918 CA. (2014). Regulation of the muscle fiber microenvironment by activated satellite cells  
919 during hypertrophy. *FASEB J* **28**, 1654-1665.  
920
- 921 Gillies AR & Lieber RL. (2011). Structure and function of the skeletal muscle extracellular matrix.  
922 *Muscle Nerve* **44**, 318-331.  
923
- 924 Girard O, Mendez-Villanueva A & Bishop D. (2011). Repeated-Sprint Ability—Part I. *Sports Med* **41**,  
925 673-694.  
926
- 927 Glaister M, Howatson G, Pattison JR & McInnes G. (2008). The reliability and validity of fatigue  
928 measures during multiple-sprint work: an issue revisited. *J Strength Cond* **22**, 1597-1601.  
929
- 930 Grohmann M, Foulstone E, Welsh G, Holly J, Shield J, Crowne E & Stewart C. (2005). Isolation and  
931 validation of human prepubertal skeletal muscle cells: maturation and metabolic effects of  
932 IGF-I, IGFBP-3 and TNF $\alpha$ . *J Physiol* **568**, 229-242.  
933
- 934 Guex K, Gojanovic B & Millet GP. (2012). Influence of hip-flexion angle on hamstrings isokinetic  
935 activity in sprinters. *Journal of athletic training* **47**, 390-395.  
936

- 937 Hermens HJ, Freriks B, Disselhorst-Klug C & Rau G. (2000). Development of recommendations for  
938 SEMG sensors and sensor placement procedures. *Journal of electromyography and*  
939 *Kinesiology* **10**, 361-374.  
940
- 941 Howatson G & Milak A. (2009). Exercise-induced muscle damage following a bout of sport specific  
942 repeated sprints. *J Strength Cond* **23**, 2419-2424.  
943
- 944 Howatson G & Van Someren KA. (2008). The prevention and treatment of exercise-induced muscle  
945 damage. *Sports Med* **38**, 483-503.  
946
- 947 Joe AW, Yi L, Natarajan A, Le Grand F, So L, Wang J, Rudnicki MA & Rossi FM. (2010). Muscle injury  
948 activates resident fibro/adipogenic progenitors that facilitate myogenesis. *Nat Cell Biol* **12**,  
949 153.  
950
- 951 Jones D, Newham D, Round J & Tolfree S. (1986). Experimental human muscle damage:  
952 morphological changes in relation to other indices of damage. *J Physiol* **375**, 435-448.  
953
- 954 Jonhagen S, Nemeth G & Eriksson E. (1994). Hamstring injuries in sprinters the role of concentric and  
955 eccentric hamstring muscle strength and flexibility. *The American Journal of Sports Medicine*  
956 **22**, 262-266.  
957
- 958 Kellis E & Baltzopoulos V. (1999). In vivo determination of the patella tendon and hamstrings  
959 moment arms in adult males using videofluoroscopy during submaximal knee extension and  
960 flexion. *Clinical Biomechanics* **14**, 118-124.  
961
- 962 Kirk EA & Rice CL. (2016). Contractile function and motor unit firing rates of the human hamstrings. *J*  
963 *Neurophysiol*, jn. 00620.02016.  
964
- 965 Lanza MB, Balshaw TG, Massey GJ & Folland JP. (2018). Does normalization of voluntary EMG  
966 amplitude to MMAX account for the influence of electrode location and adiposity? *Scand J*  
967 *Med Sci Sports*.  
968
- 969 Mackey AL, Magnan M, Chazaud B & Kjaer M. (2017). Human skeletal muscle fibroblasts stimulate in  
970 vitro myogenesis and in vivo muscle regeneration. *J Physiol* **595**, 5115-5127.  
971
- 972 Maiwald C, Sterzing T, Mayer T & Milani T. (2009). Detecting foot-to-ground contact from kinematic  
973 data in running. *Footwear Science* **1**, 111-118.  
974
- 975 Marshall PW, Lovell R, Jeppesen GK, Andersen K & Siegler JC. (2014). Hamstring muscle fatigue and  
976 central motor output during a simulated soccer match. *PLoS One* **10**, e102753.  
977
- 978 McClay I & Manal K. (1999). Three-dimensional kinetic analysis of running: significance of secondary  
979 planes of motion. *Medicine and Science in Sports and Exercise* **31**, 1629-1637.  
980
- 981 Murphy MM, Lawson JA, Mathew SJ, Hutcheson DA & Kardon G. (2011). Satellite cells, connective  
982 tissue fibroblasts and their interactions are crucial for muscle regeneration. *Development*  
983 **138**, 3625-3637.  
984
- 985 Nedelec M, McCall A, Carling C, Legall F, Berthoin S & Dupont G. (2014). The influence of soccer  
986 playing actions on the recovery kinetics after a soccer match. *J Strength Cond* **28**, 1517-1523.  
987

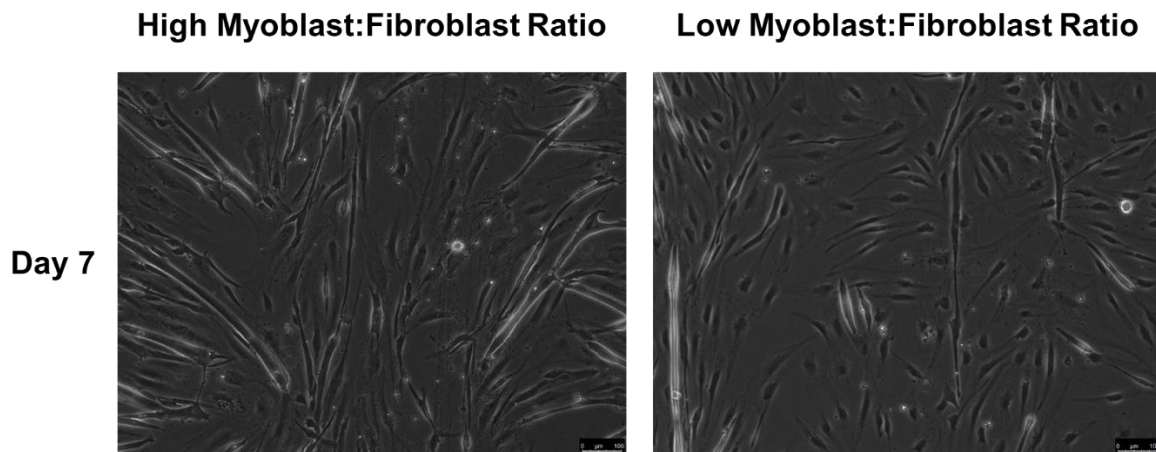
- 988 Newham D, Jones D & Clarkson P. (1987). Repeated high-force eccentric exercise: effects on muscle  
989 pain and damage. *J Appl Physiol* **63**, 1381-1386.  
990
- 991 Newham D, McPhail G, Mills K & Edwards R. (1983). Ultrastructural changes after concentric and  
992 eccentric contractions of human muscle. *J Neurol Sci* **61**, 109-122.  
993
- 994 Onishi H, Yagi R, Oyama M, Akasaka K, Ihashi K & Handa Y. (2002). EMG-angle relationship of the  
995 hamstring muscles during maximum knee flexion. *Journal of Electromyography and*  
996 *Kinesiology* **12**, 399-406.  
997
- 998 Opar DA, Williams M, Timmins R, Hickey J, Duhig S & Shield A. (2014). Eccentric hamstring strength  
999 and hamstring injury risk in Australian footballers. *Medicine & Science in Sports & Exercise* **46**.  
1000
- 1001 Opar DA, Williams MD & Shield AJ. (2012). Hamstring strain injuries. *Sports Med* **42**, 209-226.  
1002
- 1003 Owens DJ, Sharples AP, Polydorou I, Alwan N, Donovan T, Tang J, Fraser WD, Cooper RG, Morton JP &  
1004 Stewart C. (2015). A systems-based investigation into vitamin D and skeletal muscle repair,  
1005 regeneration, and hypertrophy. *Am J Physiol-Endoc M* **309**, E1019-E1031.  
1006
- 1007 Paschalis V, Giakas G, Baltzopoulos V, Jamurtas AZ, Theoharis V, Kotzamanidis C & Koutedakis Y.  
1008 (2007). The effects of muscle damage following eccentric exercise on gait biomechanics. *Gait*  
1009 *& posture* **25**, 236-242.  
1010
- 1011 Reeves ND, Narici MV & Maganaris CN. (2004). In vivo human muscle structure and function:  
1012 adaptations to resistance training in old age. *Experimental physiology* **89**, 675-689.  
1013
- 1014 Robinson MA & Vanrenterghem J. (2012). An evaluation of anatomical and functional knee axis  
1015 definition in the context of side-cutting. *Journal of biomechanics* **45**, 1941-1946.  
1016
- 1017 Schuermans J, Van Tiggelen D, Danneels L & Witvrouw E. (2014). Biceps femoris and  
1018 semitendinosus—teammates or competitors? New insights into hamstring injury  
1019 mechanisms in male football players: a muscle functional MRI study. *Br J Sports Med* **48**,  
1020 1599-1606.  
1021
- 1022 Schwartz MH & Rozumalski A. (2005). A new method for estimating joint parameters from motion  
1023 data. *Journal of biomechanics* **38**, 107-116.  
1024
- 1025 Scott J & Huskisson E. (1979). Vertical or horizontal visual analogue scales. *Ann Rheum Dis* **38**, 560.  
1026
- 1027 Seymore KD, Domire ZJ, DeVita P, Rider PM & Kulas AS. (2017). The effect of Nordic hamstring  
1028 strength training on muscle architecture, stiffness, and strength. *Eur J Appl Physiol* **117**, 943-  
1029 953.  
1030
- 1031 Stauber W, Clarkson P, Fritz V & Evans W. (1990). Extracellular matrix disruption and pain after  
1032 eccentric muscle action. *J Appl Physiol* **69**, 868-874.  
1033
- 1034 Stewart JD, Masi TL, Cumming AE, Molnar GM, Wentworth BM, Sampath K, McPherson JM & Yaeger  
1035 PC. (2003). Characterization of proliferating human skeletal muscle-derived cells in vitro:  
1036 Differential modulation of myoblast markers by TGF- $\beta$ 2. *J Cell Physio* **196**, 70-78.  
1037



- 1038 Terry EE, Zhang X, Hoffmann C, Hughes LD, Lewis SA, Li J, Wallace MJ, Riley LA, Douglas CM &  
1039 Gutierrez-Monreal MA. (2018). Transcriptional profiling reveals extraordinary diversity  
1040 among skeletal muscle tissues. *eLife* **7**.  
1041
- 1042 Thelen DG, Chumanov ES, Hoerth DM, Best TM, Swanson SC, Li L, Young M & Heiderscheidt BC. (2005).  
1043 Hamstring muscle kinematics during treadmill sprinting. *Medicine and science in sports and*  
1044 *exercise* **37**, 108-114.  
1045
- 1046 Tidball JG. (2011). Mechanisms of muscle injury, repair, and regeneration. *Comprehensive Physiology*  
1047 **1**, 2029-2062.  
1048
- 1049 Timmins RG, Bourne MN, Shield AJ, Williams MD, Lorenzen C & Opar DA. (2015). Short biceps femoris  
1050 fascicles and eccentric knee flexor weakness increase the risk of hamstring injury in elite  
1051 football (soccer): a prospective cohort study. *Br J Sports Med*, bjsports-2015-095362.  
1052
- 1053 Timmins RG, Bourne MN, Shield AJ, Williams MD, Lorenzen C & Opar DA. (2016a). Short biceps  
1054 femoris fascicles and eccentric knee flexor weakness increase the risk of hamstring injury in  
1055 elite football (soccer): a prospective cohort study. *Br J Sports Med* **50**, 1524-1535.  
1056
- 1057 Timmins RG, Opar DA, Williams MD, Schache AG, Dear NM & Shield AJ. (2014). Reduced biceps  
1058 femoris myoelectrical activity influences eccentric knee flexor weakness after repeat sprint  
1059 running. *Scandinavian journal of medicine & science in sports* **24**, e299-e305.  
1060
- 1061 Timmins RG, Shield AJ, Williams MD, Lorenzen C & Opar DA. (2016b). Architectural adaptations of  
1062 muscle to training and injury: a narrative review outlining the contributions by fascicle  
1063 length, pennation angle and muscle thickness. *Br J Sports Med*, bjsports-2015-094881.  
1064
- 1065 Turrina A, Martínez-González MA & Stecco C. (2013). The muscular force transmission system: role of  
1066 the intramuscular connective tissue. *J Bodywork Movement Ther* **17**, 95-102.  
1067
- 1068 Valle X, Alentorn-Geli E, Tol JL, Hamilton B, Garrett WE, Pruna R, Til L, Gutierrez JA, Alomar X & Balias  
1069 R. (2017). Muscle injuries in sports: a new evidence-informed and expert consensus-based  
1070 classification with clinical application. *Sports Med* **47**, 1241-1253.  
1071
- 1072 van der Horst N, Smits D-W, Petersen J, Goedhart EA & Backx FJ. (2015). The Preventive Effect of the  
1073 Nordic Hamstring Exercise on Hamstring Injuries in Amateur Soccer Players A Randomized  
1074 Controlled Trial. *The American journal of sports medicine*, 0363546515574057.  
1075
- 1076 van Dyk N, Bahr R, Whiteley R, Tol JL, Kumar BD, Hamilton B, Farooq A & Witvrouw E. (2016).  
1077 Hamstring and Quadriceps Isokinetic Strength Deficits Are Weak Risk Factors for Hamstring  
1078 Strain Injuries A 4-Year Cohort Study. *The American journal of sports medicine*,  
1079 0363546516632526.  
1080
- 1081 Verheul J, Clansey AC & Lake MJ. (2017). Adjustments with running speed reveal neuromuscular  
1082 adaptations during landing associated with high mileage running training. *Journal of applied*  
1083 *physiology* **122**, 653-665.  
1084
- 1085 Verma S, Moiz J, Shareef M & Husain M. (2015). Physical performance and markers of muscle  
1086 damage following sports specific sprints in male collegiate soccer players: repeated bout  
1087 effect. *The Journal of sports medicine and physical fitness*.  
1088

- 1089 Wang N, Tytell JD & Ingber DE. (2009). Mechanotransduction at a distance: mechanically coupling the  
1090 extracellular matrix with the nucleus. *Nature reviews Molecular cell biology* **10**, 75-82.  
1091  
1092 Woods K, Bishop P & Jones E. (2007). Warm-up and stretching in the prevention of muscular injury.  
1093 *Sports Med* **37**, 1089-1099.  
1094  
1095 Wüst RC, Morse CI, De Haan A, Jones DA & Degens H. (2008). Sex differences in contractile properties  
1096 and fatigue resistance of human skeletal muscle. *Experimental physiology* **93**, 843-850.  
1097

1098 **SUPPLEMENTARY INFORMATION**



- 1099  
1100 **Figure supplement 5** Representative images for muscle cell differentiation with a high  
1101 myoblast:fibroblast ratio (2.4; left) and with a low myoblast:fibroblast ratio (0.3; right) at day seven.  
1102 Magnification is x 10.5, and scale bar is 100  $\mu$ m.

1103

1104

- 1105 **Table supplement 4** Architectural parameters of biceps femoris long head (mean  $\pm$  SD).

Muscle length [cm]	Fascicle length [cm]	PCSA [cm <sup>2</sup> ]	Volume [cm <sup>3</sup> ]	Fascicle Pennation Angle [°]
27.86 $\pm$ 2.13	7.94 $\pm$ 1.38	23.4 $\pm$ 4.62	182.2 $\pm$ 29.5	12.7 $\pm$ 2.77

Fascicle length at 50% of BF<sub>LH</sub> muscle length; PCSA – Physiological cross-sectional area.

1106

1107 **Table supplement 6** *Linear regression analysis between the myoblast:fibroblast ratio and fusion*  
1108 *parameters at day 7 and CK activity at day 10 in vitro.*

	<b>R<sup>2</sup></b>	<b>F-Test</b>	<b>P Value</b>
Total myotubes [n]	0.345	F(1,10) = 5.27	0.045*
Myotube Length [ $\mu\text{m}$ ]	0.339	F(1,10) = 5.13	0.047*
Myotube Diameter [ $\mu\text{m}$ ]	0.387	F(1,10) = 5.56	0.031*
Myotube Area [ $\mu\text{m}^2$ ]	0.404	F(1,10) = 6.79	0.026*
CK activity [mU/mL]	0.409	F(1,10) = 6.23	0.034*

\* significant ( $P < 0.05$ );

1109